In Silico Pharmacology (2018) 6:9
https://doi.org/10.1007/s40203-018-0046-4

ORIGINAL RESEARCH

High throughput screening against pantothenate synthetase identifies amide inhibitors against *Mycobacterium tuberculosis* and *Staphylococcus aureus*

Sayantan Pradhan[1] · Chittaranjan Sinha[1]

Received: 24 March 2018 / Accepted: 10 April 2018 / Published online: 8 May 2018

Abstract

Pantothenate is a crucial enzyme for the synthesis of coenzyme A and acyl carrier protein in *Mycobacterium tuberculosis* and *Staphylococcus aureus*. It is indispensable for the growth and survival of these bacteria. Amides analogs are designed and have been used as inhibitors of pantothenate synthetase. Molecular docking approach has been used to design and predict the drug activity of molecule to the specific disease. In this work, more than hundred amides have been screened by Discovery Studio molecular docking programme to search best suitable molecule for the treatment of *Mycobacterium tuberculosis*. Pharmacophore generation has been done to recognize the binding modes of inhibitors in the receptor active site. To observe the stability and flexibility of inhibitors molecular dynamics (MD) simulation has been done; Lipinski's rule of five protocols is followed to screen drug likeness and ADMET (absorption, distribution, metabolism, excretion and toxicity) filtration is also used to value toxicity. DFT computation of optimized geometry and derivation of MOs has been used to correlate the drug likeness. The small difference in energy between HOMO and LUMO may help to activate the drug in the protein environment quickly. 2-Hydroxy-5-[(E)-2-{4-[(prop-2-enamido)sulfonyl]phenyl}diazen-1-yl]benzoic acid (M1) shows best theoretical efficiency against *Mycobacterium tuberculosis* (MTB) pantothenate synthetase and so does 2-hydroxy-5-[(E)-2-{4-[(2-phenylacetamido)sulfonyl]phenyl}diazen-1-yl]benzoic acid (M2) against *Staphylococcus aureus* pantothenate synthetase. These compounds also bind to Adenine–Thymine region of tuberculosis DNA.

Graphical abstract

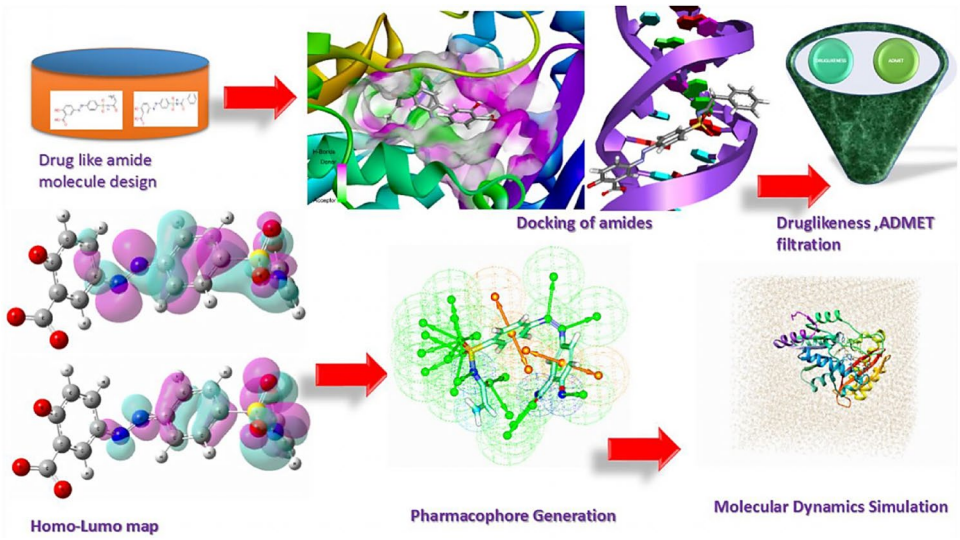

Extended author information available on the last page of the article

Keywords Pantothenate synthetase inhibitors · Heterocyclic amide compounds · Structure based drug design · Molecular docking · ADMET · MD simulation

Introduction

Virtually one-third of the human population of the world is suffering from *Mycobacterium tuberculosis* (MTB) infection (Onyango 2011). Despite the existence of approved drug against TB, it continues to claim approximately 1.5 million lives every year due to drug-resistant TB problem (multidrug resistant tuberculosis, MDR-TB and extensively drug resistant tuberculosis, XDR-TB). So, there is an urgent need to develop new anti-TB drugs (Onyango 2011). In the search for MTB vaccine, growth and virulence of pantothenate synthetase (panC) auxotrophs has been severely collaborated, sustaining the theory of the necessity of this enzyme and its prettiness as an antimicrobial target (White et al. 2007).

Pantothenate synthetase (PS) plays critical roles in many cellular processes like, fatty acid metabolism. It catalyzes the adenosine triphosphate (ATP)-dependent condensation of pantoate and β-alanine to form pantothenate (vitamin B5), and key precursor for the synthesis of coenzyme A (CoA) and acyl carrier protein (ACP) (von Delft et al. 2001). Upon action of fatty acid synthases on Acetyl-CoA and NADPH fatty acids are generated which combine with glycerol followed by phosphorylation could form phospholipid (Leonardi and Jackowski 2007). The bulk of the lipid bilayers those make up cell wall and surround the organelles within the cells have been synthesized from phospholipids (Berg et al. 2002; Chaffey et al. 2003). Lipid-rich cell wall of MTB is an essential element of intracellular survival and pathogenicity, and also thought to contribute to the difficulty of effectively delivering antimicrobial agents into the cell. The significance of this lipid-rich cell wall is underscored by the large number of genes (approximately 250) encoding enzymes in fatty acid metabolism present in the MTB genome, making this pathway a promising target for new antibacterial drug discovery (Cole et al. 1998). Indeed, several anti-tubercular agents are known to inhibit cell wall biosynthesis.

PanC is absent in mammals. It searches pantothenate from their diet using pantothenate permease, of which, there is no homolog in MTB (Table 1) (Grassl 1992; Vallari and Rock 1985). Literature search shows that MTB mutant defective in the de novo biosynthesis of pantothenate is highly attenuated in both immune compromised and immune competent mice. It points out that functionality of pantothenate in biosynthetic pathway is crucial (Fig. 1) for virulence of MTB (Wang and Eisenberg 2003). Different industries invest over 50 billion dollars on research and development each year to identify potential new drug targets. Pantothenate Synthetase may explore an opportunity to design the drug resistant TB drugs (Overington et al. 2006).

Amides are known to play a crucial role in supramolecular anion sensing technology (McMurry et al. 2017). They may also be used as antibacterial agents against Gram positive and Gram negative bacteria in the future design of drugs (Stefańska et al. 2015). Amide derivatives (Table 2) show numerous types of biological features as anthelmintic, antihistaminic, antifungal, and antibacterial including *Staphylococcus aureus* and *Mycobacterium tuberculosis* (Yildiz et al. 2008; Jagessar and Rampersaud 2007; The Sulfa Derivatives in the Treatment of Tuberculosis 1944).

On the other hand, sulfa drugs show potent anti-microbial activity and literature has shown that they are active against *Mycobacterium tuberculosis* and *Staphylococcus aureus* (Bartzatt et al. 2010; Holloway et al. 2016). In this work, a series of amide functionalized sulfa drugs have been designed by modifying sulfa drugs amides by structure based drug design. Amides have been docked to examine their action against *Mycobacterium tuberculosis* (MTB) and *Staphylococcus aureus* (SA).

According to some scientists at Lilly Research Laboratories, Eli Lilly & Company, USA two compounds with 4-cyano-1-methyl-3-(4-phenylphenyl)pyrrole-2-carboxylic acid core structure, inhibited MTB pantothenate synthetase (Kumar et al. 2013).The MIC_{50} values of the two compounds were high (55 and 118 μM. This suggested the growth inhibitory properties were due to PanC-mediated inhibition[a].The IUPAC name of the compounds are 3-{[1,1′-biphenyl]-4-yl}-4-cyano-5-(ethylsulfanyl)-1-methyl-1H-pyrrole-2-carboxylic acid (compound 1) and 3-{[1,1′-biphenyl]-4-yl}-4-cyano-5-ethyl-1-methyl-1H-pyrrole-2-carboxylic acid (compound 2). In the present work it has been showed that 2-hydroxy-5-[(E)-2-{4-[(prop-2-enamido)sulfonyl]phenyl}diazen-1-yl]benzoic acid and 2-hydroxy-5-[(E)-2-{4-[(2-phenylacetamido)sulfonyl]phenyl}diazen-1-yl]benzoic acid showed better docking score than compound 1 (C1) and compound 2 (C2). Sulfonamide, sulfamoyl groups as co-crystalized structure in the crystal structure of pantothenate synthetase proves their efficiency in binding and inhibition.

Out of 154 different amides of sulfa drugs 93 derivatives show higher docking score (binding affinity) than C1 (Table 3). For SA also some compounds exhibit docking score higher than C2 (Table 4) which are used to treat bacterial infection by susceptible microorganisms (Kumar et al. 2013; Wu et al. 2003). Molecular dynamics (MD) simulations have been done to observe the effect of explicit solvent molecules on protein (Pantothenate Synthetase) ligand (amides) complex structure and stability to achieve

time-averaged attributes of the bimolecular system, along with diverse thermodynamic parameters. Drug likeness has been examined following Lipinski's rule of five filter (Lipinski et al. 2001). The molecular orbitals are used to calculate the electronic configuration, molecular reactivity and stability of the compounds by density functional theory (DFT) computational process (Rozhenko 2014). Pharmacophore map generation has also done to observe steric and electronic features of best docked amides that ensured the optimal interactions with a receptor (Pantothenate Synthetase) and to block its biological response (Wermuth et al. 1998). ADMET (absorption, distribution, metabolism, excretion and toxicity) filtration has been applied to check toxicity of the compounds (Hou and Wang 2008). Two compounds out of 154 amides, 2-hydroxy-5-[(E)-2-{4-[(prop-2-enamido) sulfonyl]phenyl} diazen-1-yl]benzoic acid (**M1**, Table 2) and 2-hydroxy-5-[(E)-2-{4-[(2-phenylacetamido)sulfonyl] phenyl}diazen-1-yl]benzoic acid (**M2**, Table 2) exhibit better theoretical drug potency than approved and have crossed ADMET and Lipinski's rule of five filter (Table 2). These two compounds also bind to Adenine–Thymine region of tuberculosis DNA (Sirajuddin et al. 2013).

Methods and materials

Sequence alignment analysis

Functional similarity between two or more sequences of amino acids has been carried out by using *in silico* multiple-sequence alignment (MSA) and is important for finding the functionality of proteins and evolution history of the species (Nguyen and Pan 2013).

High throughput virtual screening (HTVS)

Structure-based drug discovery is a vital process for fast and cost-effective lead discovery and proven to be more efficient than the conventional wet lab drug discovery (Lionta et al. 2014; Pradhan and Sinha 2017). High-Throughput Screening (HTS) is an approach to drug discovery that has become a standard tool for structure-based drug discovery. It is basically a process of screening of large number of drug like molecules against selected and specific drug targets. HTS are used for screening of various types of libraries, including combinatorial chemistry, genomics, protein, and peptide libraries (Szymański et al. 2012).

Drug-like amide molecule preparation

We have collected 154 small Lipinski's filter passed amide molecule compounds from the PubChem database which inhibit pantothenate synthetase enzyme (Database Resources

Table 1 Percent identity matrix (PAM) for searching similarities between different species containing Pantothenate synthetase

Seq. no.	PDB chain	Species	Similarities in percentage											
1	3N8H_A|PDB|CHAIN|SEQUENCE	*Francisellatularensis*	100	36.4	39.46	38.52	37.93	35.57	38.67	34.24	34.4	37.26	38.58	36.29
2	4EFK_A|PDB|CHAIN|SEQUENCE	*Mycobacterium tuberculosis*	36.4	100	43.93	43.84	41.79	43.96	45.71	39.21	44.81	41.08	40.36	36.43
3	3Q10_A|PDB|CHAIN|SEQUENCE	*Yersinia pestis*	39.46	43.93	100	71.73	72.82	44.96	50.18	40.57	45.42	44.91	44.24	38.87
4	1IHO_A|PDB|CHAIN|SEQUENCE	*Escherichia coli*	38.52	43.84	71.73	100	87.99	44.73	52.16	40.71	46.89	45.55	46.76	40.5
5	3MUE_A|PDB|CHAIN|SEQUENCE	*Salmonella enterica*	37.93	41.79	72.82	87.99	100	41.01	49.47	39.86	45.42	44.56	43.88	40.28
6	3UK2_A|PDB|CHAIN|SEQUENCE	*Burkholderiathailandensis*	35.57	43.96	44.96	44.73	41.01	100	54.48	40.73	44.78	45.88	44.53	37.32
7	5KWV_A|PDB|CHAIN|SEQUENCE	*Neisseria gonorrhoeae*	38.67	45.71	50.18	52.16	49.47	54.48	100	37.91	46.1	43.86	46.72	38.49
8	3AG6_A|PDB|CHAIN|SEQUENCE	*Staphylococcus aureus*	34.24	39.21	40.57	40.71	39.86	40.73	37.91	100	41.82	43.11	45.71	42.91
9	1UFV_A|PDB|CHAIN|SEQUENCE	*Thermusthermophilus*	34.4	44.81	45.42	46.89	45.42	44.78	46.1	41.82	100	50.91	51.09	40.15
10	3INN_A|PDB|CHAIN|SEQUENCE	*Brucellamelitensis*	37.26	41.08	44.91	45.55	44.56	45.88	43.86	43.11	50.91	100	50.36	41.05
11	2EJC_A|PDB|CHAIN|SEQUENCE	*Thermotoga maritima*	38.58	40.36	44.24	46.76	43.88	44.53	46.72	45.71	51.09	50.36	100	52.33
12	3MXT_A|PDB|CHAIN|SEQUENCE	*Campylobacter jejuni*	36.29	36.43	38.87	40.5	40.28	37.32	38.49	42.91	40.15	41.05	52.33	100

of the National Center for Biotechnology Information 2013). The compounds are drawn by compiling sulfa drugs with amides attached to the amino group of sulfa drugs by Accelrys Draw v4. The 3D coordinates and change of ionization are done by Discovery Studio 4 software's ligand preparation wizard. Compounds are prepared using the "Prepare Ligand" protocol in Discovery Studio v4; default parameters towards performing the CDOCKER simulation with sdf files (The Sulfa Derivatives in the Treatment of Tuberculosis 1944).

a. Docking preparation of pantothenate synthetase

Pantothenate synthetase of MTB has been retrieved from RCSB PDB database with five bound-inhibitors. The protein data bank (pdb) file (pdb id: 4efk) showed a dimer of two chains. However, in the present study, only the monomeric unit (A-chain) has been used in the docking studies because it has two N, N-dimethylthiophene-3-sulfonamide bound inhibitors. The pantothenate synthetase of SA was retrieved from RCSB PDB with three bound-inhibitors (pdb id: 3ag6). The pdb file was a dimer of two chains, only the monomeric unit (A- chain) was used in the docking studies.

The bounded inhibitors from the pdb structure are removed before docking. Prepare Protein protocol has been executed such as inserting missing atoms in incomplete residues, modeling missing loop regions, and removing waters from protein. The default parameter values are mostly kept the invariant in the Prepare Protein protocol of Discovery Studio 4.

b. Molecular docking

Molecular docking of 154 selected pantothenate synthetase inhibitors to the receptor enzyme has been carried out in the present study by using CDOCKER with Discovery Studio v4. To perform flexible docking, for the small-molecules all torsion angles are set to be free. CDOCKER is a powerful CHARMm-based docking method that has been used to generate highly accurate docked poses. In this refinement application, the ligands were conceded to tilt around the rigid receptor (Wu et al. 2003). In the CDOCKER simulation the following parameters are used: top hits-10, random conformations-10, orientations to refine-10, and force field-CHARMm. For the assurance of potential relationships between pantothenate synthetase and amides, predicted CDOCKER energy values of the best docked conformations of small-molecule inhibitors (amides and approved drugs) are selected as preliminary binding conformations and saved for observing interactions between pantothenate synthetase and amides.

Drug likeness

Lipinski's rule of five (RO5) describes four simple physicochemical factors ranges (MWT < 500, log P < 5, H-bond donors < 5, H bond acceptors < 10) related with 90% of orally active drugs that have accomplished phase II clinical status (Lipinski et al. 2001). These physicochemical factors are related with aqueous solubility, intestinal permeability

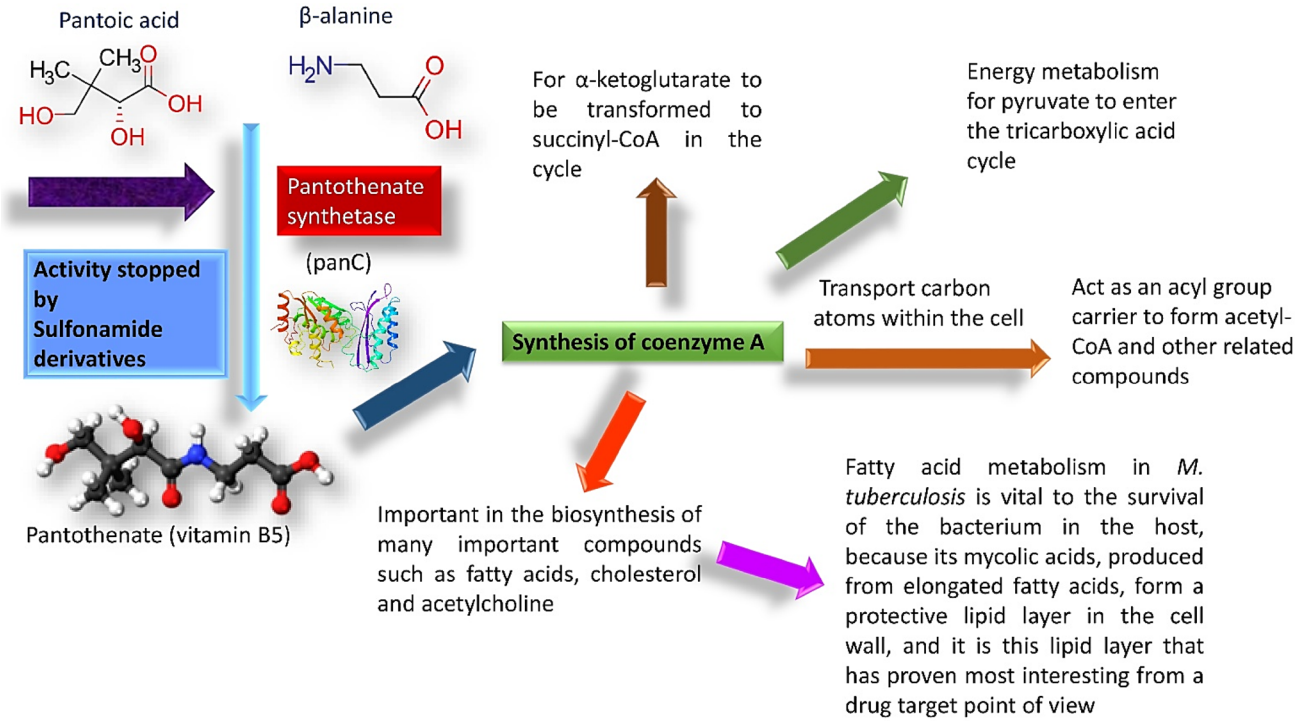

Fig. 1 Activity of pantothenate synthetase

Table 2 Selected amides (IUPAC names are given) showing docking score (CDOCKER energy) against Mycobacterial and *Staphylococcus* p.s. They have been passed the Lipinski's rule and ADMET filter

	IUPAC name of amides	MTB	SA	Lipinski's rule	ADMET
A	*Sulfamethoxazole*	a.u.	a.u.		
1	(2S)-2-amino-4-({4-[(5-methyl-1,2-oxazol-3-yl)sulfamoyl]phenyl}carbamoyl)butanoic acid	− 44.63	− 46.94	+	+
2	(2S)-2-amino-*N*-{4-[(5-methyl-1,2-oxazol-3-yl)sulfamoyl]phenyl}-3-phenylpropanamide	− 46.53	− 55.40	+	+
3	2-Amino-*N*-{4-[(5-methyl-1,2-oxazol-3-yl)sulfamoyl]phenyl}benzamide	− 45.32	− 47.30	+	+
4	2-Hydroxy-*N*-{4-[(5-methyl-1,2-oxazol-3-yl)sulfamoyl]phenyl}benzamide	− 56.43	− 53.08	+	+
5	4-({4-[(5-Methyl-1,2-oxazol-3-yl)sulfamoyl]phenyl}amino)benzene-1-sulfonamide	− 48.41	− 48.83	+	+
6	4-({4-[(5-Methyl-1,2-oxazol-3-yl)sulfamoyl]phenyl}amino)benzene-1-sulfonamide	− 50.02	− 50.64	+	+
7	4-Methyl-*N*-{4-[(5-methyl-1,2-oxazol-3-yl)sulfamoyl]phenyl}benzene-1-sulfonamide	− 40.11	− 47.32	+	+
8	5-({4-[(5-Methyl-1,2-oxazol-3-yl)sulfamoyl]phenyl}amino)naphthalene-1-sulfonamide	− 35.012	− 52.06	+	+
9	6-({4-[(5-Methyl-1,2-oxazol-3-yl)sulfamoyl]phenyl}amino)pyridine-3-carboxamide	− 50.57	− 48.74	+	+
10	*N*-{4-[(5-methyl-1,2-oxazol-3-yl)sulfamoyl]phenyl}acetamide	− 37.12	− 36.75	+	+
11	*N*-{4-[(5-methyl-1,2-oxazol-3-yl)sulfamoyl]phenyl}benzamide	− 45.62	− 46.02	+	+
12	*N*-{4-[(5-methyl-1,2-oxazol-3-yl)sulfamoyl]phenyl}hexanamide	− 41.38	− 49.40	+	+
13	*N*-(5-methyl-1,2-oxazol-3-yl)-4-(*N*-methylhydrazido)benzene-1-sulfonamide	ND	− 55.37	+	+
14	4-(*N*-butylbenzenesulfonamido)-*N*-(5-methyl-1,2-oxazol-3-yl)benzene-1-sulfonamide	− 38.70	− 38.31	+	+
15	*N*-{4-[(5-methyl-1,2-oxazol-3-yl)sulfamoyl]phenyl}prop-2-enamide	− 38.21	− 35.20	+	+
16	*N*-{4-[(5-methyl-1,2-oxazol-3-yl)sulfamoyl]phenyl}pyrazine-2-carboxamide	− 45.32	− 46.67	+	+
17	*N*-{4-[(5-methyl-1,2-oxazol-3-yl)sulfamoyl]phenyl}pyridine-3-carboxamide	ND	− 47.12	+	+
18	(2R)-4-carbamoyl-2-({4-[(5-methyl-1,2-oxazol-3-yl)sulfamoyl]phenyl}amino)butanoic acid	− 53.47	− 57.71	+	+
19	(2R,3S)-*N*-{4-[(5-methyl-1,2-oxazol-3-yl)sulfamoyl]phenyl}-3-[(4E,7E)-nona-4,7-dienoyl]oxirane-2-carboxamide	− 44.86	− 62.80	+	+
20	(2S)-2,6-diamino-*N*-{4-[(5-methyl-1,2-oxazol-3-yl)sulfamoyl]phenyl}hexanamide	− 50.59	− 52.40	+	+
21	*N*-{4-[(5-methyl-1,2-oxazol-3-yl)sulfamoyl]phenyl}-1,3-benzothiazole-2-sulfonamide	− 40.30	− 49.45	+	+
22	*N*-{4-[(5-methyl-1,2-oxazol-3-yl)sulfamoyl]phenyl}-1,3-thiazole-2-sulfonamide	− 41.62	− 45.85	+	+
23	*N*-{4-[(5-methyl-1,2-oxazol-3-yl)sulfamoyl]phenyl}-2,3-dihydro-1H-indene-5-sulfonamide	41.73	− 47.61	+	+
24	*N*-{4-[(5-methyl-1,2-oxazol-3-yl)sulfamoyl]phenyl}-2-phenoxyacetamide	− 42.48	− 49.78	+	+
25	3-Amino-*N*-{4-[(5-methyl-1,2-oxazol-3-yl)sulfamoyl]phenyl}benzamide	− 48.74	− 49.06	+	+
26	*N*-(4-ethoxyphenyl)-*N*-{4-[(5-methyl-1,2-oxazol-3-yl)sulfamoyl]phenyl}acetamide	− 44.95	− 50.17	+	+
27	*N*-methyl-*N*-{4-[(5-methyl-1,2-oxazol-3-yl)sulfamoyl]phenyl}acetamide	− 38.90	− 39.89	+	+
28	*N*-{4-[(5-methyl-1,2-oxazol-3-yl)sulfamoyl]phenyl}thiophene-2-sulfonamide	− 38.80	− 42.56	+	+
29	*N*-{4-[(5-methyl-1,2-oxazol-3-yl)sulfamoyl]phenyl}-1,2,3,4-tetrahydroisoquinoline-7-sulfonamide	− 45.4053	− 49.9116	+	+
30	1-Methyl-*N*-{4-[(5-methyl-1,2-oxazol-3-yl)sulfamoyl]phenyl}-3-oxo-1,3-dihydro-2,1-benzothiazole-5-sulfonamide	− 42.03	− 56.77	+	+
31	*N*-{4-[(5-methyl-1,2-oxazol-3-yl)sulfamoyl]phenyl}-2-propylpentanamide	− 42.87	− 48.82	+	+
32	*N*-{4-[(5-methyl-1,2-oxazol-3-yl)sulfamoyl]phenyl}-3-oxo-*N*-[(3S)-2-oxooxolan-3-yl]octanamide	ND	− 63.91	+	+
33	*N*-[2-({4-[(5-methyl-1,2-oxazol-3-yl)sulfamoyl]phenyl}amino)ethyl]isoquinoline-5-sulfonamide	ND	− 37.33	+	+
34	*N*-{4-[(5-methyl-1,2-oxazol-3-yl)sulfamoyl]phenyl}-2-oxopropanamide	− 42.18	− 40.96	+	+
35	4-(4-Chlorophenyl)-*N*-{4-[(5-methyl-1,2-oxazol-3-yl)sulfamoyl]phenyl}piperazine-1-carboximidamide	ND	ND	+	+
36	4-Amino-*N*-{4-[(5-methyl-1,2-oxazol-3-yl)sulfamoyl]phenyl}-1H-imidazole-5-carboxamide	− 43.80	− 41.97	+	+
37	5-Hydroxy-*N*-{4-[(5-methyl-1,2-oxazol-3-yl)sulfamoyl]phenyl}naphthalene-1-sulfonamide	− 39.17	− 51.45	+	+
38	4-Benzenesulfonamido-*N*-(5-methyl-1,2-oxazol-3-yl)benzene-1-sulfonamide	− 43.03	− 46.33	+	+

Table 2 (continued)

	IUPAC name of amides	MTB	SA	Lipinski's rule	ADMET
39	4-Hydroxy-3-methoxy-*N*-{4-[(5-methyl-1,2-oxazol-3-yl)sulfamoyl]phenyl}benzamide	− 48.55	− 70.46	+	+
40	*N*-{4-[(5-methyl-1,2-oxazol-3-yl)sulfamoyl]phenyl}-*N*-phenyl-1H-pyrazole-5-carboxamide	− 48.013	− 50.82	+	+
41	*N*-{4-[(5-methyl-1,2-oxazol-3-yl)sulfamoyl]phenyl}-*N*-phenylformamide	− 38.78	− 44.14	+	+
42	*N*-{4-[(5-methyl-1,2-oxazol-3-yl)sulfamoyl]phenyl}piperidine-1-sulfonamide	− 41.12	− 49.65	+	+
43	4-[(1,2-Benzoxazol-3-yl)methanesulfonamido]-*N*-(5-methyl-1,2-oxazol-3-yl)benzene-1-sulfonamide	− 41.82	− 49.84	+	+
44	*N*-{4-[(5-methyl-1,2-oxazol-3-yl)sulfamoyl]phenyl}-1-benzothiophene-2-sulfonamide	− 43.82	− 9.82	+	+
45	4-(*N*-{4-[(5-methyl-1,2-oxazol-3-yl)sulfamoyl]phenyl}acetamido)benzoic acid	− 34.11	− 50.71	+	+
46	(2R)-2-[(*N*-hydroxyformamido)methyl]-4-methyl-*N*-{4-[(5-methyl-1,2-oxazol-3-yl)sulfamoyl]phenyl}pentanamide	ND	− 59.30	+	+
47	1,3-Dimethyl-*N*-{4-[(5-methyl-1,2-oxazol-3-yl)sulfamoyl]phenyl}-2-oxo-2,3-dihydro-1H-1,3-benzodiazole-5-carboxamide	− 46.39	ND	+	+
B	*Sulfadiazine*				
48	(2S)-4-carbamoyl-2-({4-[(pyrimidin-2-yl)sulfamoyl]phenyl}amino)butanoic acid	− 48.54	− 65.49	+	−
49	(2S)-2-amino-3-phenyl-*N*-{4-[(pyrimidin-2-yl)sulfamoyl]phenyl}propanamide	− 46.06	− 52.08	+	+
50	2-Amino-*N*-{4-[(pyrimidin-2-yl)sulfamoyl]phenyl}benzamide	− 44.51	− 43.50	+	+
51	2-Hydroxy-*N*-{4-[(pyrimidin-2-yl)sulfamoyl]phenyl}benzamide	− 46.65	− 44.73	+	−
52	2-Phenyl-*N*-{4-[(pyrimidin-2-yl)sulfamoyl]phenyl}acetamide	− 43.36	− 46.87	+	+
53	4-Amino-*N*-{4-[(pyrimidin-2-yl)sulfamoyl]phenyl}benzene-1-sulfonamide	− 41.56	− 48.64	+	+
54	4-Methyl-*N*-{4-[(pyrimidin-2-yl)sulfamoyl]phenyl}benzene-1-sulfonamide	− 47.37	− 49.44	+	+
55	6-({4-[(Pyrimidin-2-yl)sulfamoyl]phenyl}amino)pyridine-3-carboxamide	− 35.78	− 51.18	+	+
56	*N*-{4-[(pyrimidin-2-yl)sulfamoyl]phenyl}acetamide	− 35.78	− 37.34	+	+
57	*N*-{4-[(pyrimidin-2-yl)sulfamoyl]phenyl}benzamide	− 46.84	− 45.60	+	+
58	*N*-{4-[(pyrimidin-2-yl)sulfamoyl]phenyl}hexanamide	− 46.99	− 47.66	+	+
59	*N*-{4-[(pyrimidin-2-yl)sulfamoyl]phenyl}formamide	− 46.02	− 37.80	+	+
60	4-(*N*-butylbenzenesulfonamido)-*N*-(pyrimidin-2-yl)benzene-1-sulfonamide	− 37.22	− 50.71	+	+
61	*N*-{4-[(pyrimidin-2-yl)sulfamoyl]phenyl}prop-2-enamide	− 38.178	− 38.06	+	+
62	*N*-{4-[(pyrimidin-2-yl)sulfamoyl]phenyl}pyrazine-2-carboxamide	− 43.31	− 45.02	+	+
63	*N*-{4-[(pyrimidin-2-yl)sulfamoyl]phenyl}pyridine-3-carboxamide	− 45.56	− 44.12	+	+
64	(2R,3S)-3-[(4E,7E)-nona-4,7-dienoyl]-*N*-{4-[(pyrimidin-2-yl)sulfamoyl]phenyl}oxirane-2-carboxamide	ND	− 61.01	+	−
65	(2S)-2,6-diamino-*N*-{4-[(pyrimidin-2-yl)sulfamoyl]phenyl}hexanamide	− 51.11	− 54.59	+	−
66	*N*-{4-[(pyrimidin-2-yl)sulfamoyl]phenyl}-1,3-benzothiazole-2-sulfonamide	− 48.19	− 47.25	+	+
67	*N*-{4-[(pyrimidin-2-yl)sulfamoyl]phenyl}-1,3-thiazole-2-sulfonamide	− 40.52	− 43.90	+	+
68	2-Phenoxy-*N*-{4-[(pyrimidin-2-yl)sulfamoyl]phenyl}acetamide	− 49.30	− 48.70	+	+
69	3-Amino-*N*-{4-[(pyrimidin-2-yl)sulfamoyl]phenyl}benzamide	− 47.69	− 49.00	+	+
70	(2R)-4-carbamoyl-2-({4-[(pyrimidin-2-yl)sulfamoyl]phenyl}amino)butanoic acid	− 53.28	− 60.18	+	−
71	*N*-(4-ethoxyphenyl)-*N*-{4-[(pyrimidin-2-yl)sulfamoyl]phenyl}acetamide	− 41.89	− 52.01	+	+
72	*N*-{4-[(pyrimidin-2-yl)sulfamoyl]phenyl}acetamide	− 35.78	− 37.34	+	+
73	*N*-{4-[(pyrimidin-2-yl)sulfamoyl]phenyl}thiophene-2-sulfonamide	− 42.40	− 43.95	+	+
74	*N*-{4-[(pyrimidin-2-yl)sulfamoyl]phenyl}-1,2,3,4-tetrahydroisoquinoline-7-sulfonamide	− 44.78	− 52.40	+	+
75	1-Methyl-3-oxo-*N*-{4-[(pyrimidin-2-yl)sulfamoyl]phenyl}-1,3-dihydro-2,1-benzothiazole-5-sulfonamide	− 40.17	− 43.95	+	−
76	2-Propyl-*N*-{4-[(pyrimidin-2-yl)sulfamoyl]phenyl}pentanamide	− 45.87	− 52.11	+	−
77	3-Oxo-*N*-[(3S)-2-oxooxolan-3-yl]-*N*-{4-[(pyrimidin-2-yl)sulfamoyl]phenyl}octanamide	− 41.03	− 56.66	+	−
78	2-Oxo-*N*-{4-[(pyrimidin-2-yl)sulfamoyl]phenyl}propanamide	ND	− 41.98	+	−
79	4-(4-Chlorophenyl)-*N*-{4-[(pyrimidin-2-yl)sulfamoyl]phenyl}piperazine-1-carboximidamide	− 42.016	− 49.23	+	+
80	4-Amino-*N*-{4-[(pyrimidin-2-yl)sulfamoyl]phenyl}-1H-imidazole-5-carboxamide	− 38.34	− 47.26	+	+

Table 2 (continued)

	IUPAC name of amides	MTB	SA	Lipinski's rule	ADMET
81	5-Hydroxy-*N*-{4-[(pyrimidin-2-yl)sulfamoyl]phenyl}naphthalene-1-sulfonamide	− 43.3	− 46.86	+	−
82	4-Benzenesulfonamido-*N*-(pyrimidin-2-yl)benzene-1-sulfonamide	− 44.59	− 45.62	+	+
83	*N*-ethyl-4-hydroxy-3-methoxy-*N*-{4-[(pyrimidin-2-yl)sulfamoyl]phenyl}benzamide	− 40.13	− 49.39	+	−
84	*N*-phenyl-*N*-{4-[(pyrimidin-2-yl)sulfamoyl]phenyl}-1H-pyrazole-5-carboxamide	− 48.63	− 43.00	+	+
85	*N*-phenyl-*N*-{4-[(pyrimidin-2-yl)sulfamoyl]phenyl}formamide	ND	− 51.9081	+	+
86	*N*-{4-[(pyrimidin-2-yl)sulfamoyl]phenyl}piperidine-1-sulfonamide	− 39.31	− 47.16	+	+
87	4-[(1,2-Benzoxazol-3-yl)methanesulfonamido]-*N*-(pyrimidin-2-yl)benzene-1-sulfonamide	− 45.79	− 48.93	+	+
88	*N*-{4-[(pyrimidin-2-yl)sulfamoyl]phenyl}-1-benzothiophene-2-sulfonamide	− 41.86	− 49.57	+	+
89	4-(*N*-{4-[(pyrimidin-2-yl)sulfamoyl]phenyl}acetamido)benzoic acid	− 48.16	− 50.66	+	+
90	(2R)-2-[(*N*-hydroxyformamido)methyl]-4-methyl-*N*-{4-[(pyrimidin-2-yl)sulfamoyl]phenyl}pentanamide	ND	− 51.64	+	+
91	1,3-Dimethyl-2-oxo-*N*-{4-[(pyrimidin-2-yl)sulfamoyl]phenyl}-2,3-dihydro-1H-1,3-benzodiazole-5-carboxamide	− 19.93	− 46.00	+	+
C	*Sulfadoxine*				
92	(2S)-4-carbamoyl-2-({4-[(5,6-dimethoxypyrimidin-4-yl)sulfamoyl]phenyl}amino)butanoic acid	ND	ND	+	−
93	(2S)-2-amino-*N*-{4-[(5,6-dimethoxypyrimidin-4-yl)sulfamoyl]phenyl}-3-phenylpropanamide	− 40.08	ND	+	−
94	2-Amino-*N*-{4-[(5,6-dimethoxypyrimidin-4-yl)sulfamoyl]phenyl}benzamide	− 41.83	− 49.59	+	−
95	*N*-{4-[(5,6-dimethoxypyrimidin-4-yl)sulfamoyl]phenyl}-2-hydroxybenzamide	ND	− 71.28	+	−
96	*N*-{4-[(5,6-dimethoxypyrimidin-4-yl)sulfamoyl]phenyl}-2-phenylacetamide	− 44.46	− 48.99	+	−
97	4-Amino-*N*-{4-[(5,6-dimethoxypyrimidin-4-yl)sulfamoyl]phenyl}benzene-1-sulfonamide	− 44.53	− 53.77	+	−
98	*N*-{4-[(5,6-dimethoxypyrimidin-4-yl)sulfamoyl]phenyl}-4-methylbenzene-1-sulfonamide	− 44.03	ND	+	−
99	6-({4-[(5,6-Dimethoxypyrimidin-4-yl)sulfamoyl]phenyl}amino)pyridine-3-carboxamide	− 43.82	ND	+	−
100	*N*-{4-[(5,6-dimethoxypyrimidin-4-yl)sulfamoyl]phenyl}acetamide	− 41.15	− 42.00	+	−
101	*N*-{4-[(5,6-Dimethoxypyrimidin-4-yl)sulfamoyl]phenyl}benzamide	− 46.17	ND	+	−
102	*N*-{4-[(5,6-dimethoxypyrimidin-4-yl)sulfamoyl]phenyl}hexanamide	− 42.91	− 51.01	+	−
103	*N*-{4-[(5,6-dimethoxypyrimidin-4-yl)sulfamoyl]phenyl}formamide	− 47.49	− 40.98	+	−
104	*N*-{4-[(5,6-dimethoxypyrimidin-4-yl)sulfamoyl]phenyl}prop-2-enamide	ND	− 44.25	+	−
105	*N*-{4-[(5,6-dimethoxypyrimidin-4-yl)sulfamoyl]phenyl}pyrazine-2-carboxamide	− 47.52	ND	+	−
106	*N*-{4-[(5,6-dimethoxypyrimidin-4-yl)sulfamoyl]phenyl}pyridine-3-carboxamide	− 46.09	− 51.93	+	−
107	(2R)-4-carbamoyl-2-({4-[(5,6-dimethoxypyrimidin-4-yl)sulfamoyl]phenyl}amino)butanoic acid	ND	ND	+	−
108	(2S)-2,6-diamino-*N*-{4-[(5,6-dimethoxypyrimidin-4-yl)sulfamoyl]phenyl}hexanamide	− 46.87	ND	+	−
109	*N*-{4-[(5,6-dimethoxypyrimidin-4-yl)sulfamoyl]phenyl}-1,3-thiazole-2-sulfonamide	ND	ND	+	−
110	*N*-{4-[(5,6-dimethoxypyrimidin-4-yl)sulfamoyl]phenyl}-2-phenoxyacetamide	− 47.79	− 56.89	+	−
111	3-Amino-*N*-{4-[(5,6-dimethoxypyrimidin-4-yl)sulfamoyl]phenyl}benzamide	− 52.91	− 50.61	+	−
112	1-{4-[(5,6-Dimethoxypyrimidin-4-yl)sulfamoyl]phenyl}-3-(4-ethoxyphenyl)urea	ND	ND	+	−
113	*N*-{4-[(5,6-dimethoxypyrimidin-4-yl)sulfamoyl]phenyl}-*N*-methylacetamide	ND	− 47.15	+	−
114	*N*-{4-[(5,6-dimethoxypyrimidin-4-yl)sulfamoyl]phenyl}thiophene-2-sulfonamide	ND	− 50.31	+	−
115	4-Amino-*N*-{4-[(5,6-dimethoxypyrimidin-4-yl)sulfamoyl]phenyl}-1H-imidazole-5-carboxamide	NA	NA	−	NA
116	*N*-{4-[(5,6-dimethoxypyrimidin-4-yl)sulfamoyl]phenyl}-2-oxopropanamide	− 46.87	− 46.82	+	−
117	*N*-{4-[(5,6-dimethoxypyrimidin-4-yl)sulfamoyl]phenyl}-2-propylpentanamide	ND	− 53.05	+	+
118	4-Amino-*N*-{4-[(5,6-dimethoxypyrimidin-4-yl)sulfamoyl]phenyl}-1H-imidazole-5-carboxamide	NA	NA	−	NA
119	4-Benzenesulfonamido-*N*-(5,6-dimethoxypyrimidin-4-yl)benzene-1-sulfonamide	− 53.75	− 51.50	−	−

Table 2 (continued)

	IUPAC name of amides	MTB	SA	Lipinski's rule	ADMET
120	*N*-{4-[(5,6-dimethoxypyrimidin-4-yl)sulfamoyl]phenyl}-*N*-phenyl-1H-pyrazole-5-carboxamide	ND	ND	–	NA
121	*N*-{4-[(5,6-dimethoxypyrimidin-4-yl)sulfamoyl]phenyl}-*N*-phenylformamide	– 41.87	– 53.59	+	+
122	*N*-{4-[(5,6-dimethoxypyrimidin-4-yl)sulfamoyl]phenyl}piperidine-1-sulfonamide	ND	ND	–	–
123	4-(*N*-{4-[(5,6-dimethoxypyrimidin-4-yl)sulfamoyl]phenyl}acetamido)benzoic acid	ND	ND	–	NA
124	(2R)-*N*-{4-[(5,6-dimethoxypyrimidin-4-yl)sulfamoyl]phenyl}-2-[(*N*-hydroxyformamido)methyl]-4-methylpentanamide	ND	ND	–	NA
D	*Sulfasalaine*				
125	5-[(E)-2-(4-{[(1S)-3-carbamoyl-1-carboxypropyl]sulfamoyl}phenyl)diazen-1-yl]-2-hydroxybenzoic acid	ND	ND	–	–
126	5-[(E)-2-(4-{[(2S)-2-amino-3-phenylpropanamido]sulfonyl}phenyl)diazen-1-yl]-2-hydroxybenzoic acid	ND	– 83.98	+	+
127	5-[(E)-2-(4-{[(2-aminophenyl)formamido]sulfonyl}phenyl)diazen-1-yl]-2-hydroxybenzoic acid	– 47.53	– 82.68	+	–
128	2-Hydroxy-5-[(E)-2-(4-{[(2-hydroxyphenyl)formamido]sulfonyl}phenyl)diazen-1-yl]benzoic acid	– 47.56	– 60.56	+	–
129	2-Hydroxy-5-[(E)-2-{4-[(2-phenylacetamido)sulfonyl]phenyl}diazen-1-yl]benzoic acid (**M2**)	– 62.18	**– 85.41**	+	+
130	2-Hydroxy-5-[(E)-2-{4-[(4-methylbenzenesulfonyl)sulfamoyl]phenyl}diazen-1-yl]benzoic acid	– 54.11	– 68.96	+	–
131	5-[(E)-2-[4-(acetamidosulfonyl)phenyl]diazen-1-yl]-2-hydroxybenzoic acid	– 50.51	– 57.42	+	+
132	2-Hydroxy-5-[(E)-2-[4-(phenylformamido)sulfonylphenyl]diazen-1-yl]benzoic acid	– 46.29	– 58.41	+	+
133	5-[(E)-2-[4-(hexanamidosulfonyl)phenyl]diazen-1-yl]-2-hydroxybenzoic acid	– 42.93	– 81.40	+	+
134	2-Hydroxy-5-[(E)-2-(4-formamidosulfonylphenyl)diazen-1-yl]benzoic acid	– 61.32	– 74.46	+	+
135	2-Hydroxy-5-[(E)-2-{4-[(prop-2-enamido)sulfonyl]phenyl}diazen-1-yl]benzoic acid (**M1**)	**– 66.41**	– 70.68	+	+
136	2-Hydroxy-5-[(E)-2-(4-{[(pyridin-3-yl)formamido]sulfonyl}phenyl)diazen-1-yl]benzoic acid	– 68.67	– 66.03	+	–
137	5-[(E)-2-{4-[(4-aminobenzenesulfonyl)sulfamoyl]phenyl}diazen-1-yl]-2-hydroxybenzoic acid	NA	NA	–	NA
138	2-Hydroxy-5-[(E)-2-{4-[(4-methylbenzenesulfonyl)sulfamoyl]phenyl}diazen-1-yl]benzoic acid	NA	NA	–	NA
139	2-Hydroxy-5-[(E)-2-(4-{[(pyrazin-2-yl)formamido]sulfonyl}phenyl)diazen-1-yl]benzoic acid	NA	NA	+	NA
140	2-Hydroxy-5-[(E)-2-{4-[(2-phenoxyacetamido)sulfonyl]phenyl}diazen-1-yl]benzoic acid	– 62.84	– 79.97	+	–
141	5-[(E)-2-(4-{[(3-aminophenyl)formamido]sulfonyl}phenyl)diazen-1-yl]-2-hydroxybenzoic acid	– 56.08	– 77.70	+	+
142	5-[(E)-2-(4-{[*N*-(4-ethoxyphenyl)acetamido]sulfonyl}phenyl)diazen-1-yl]-2-hydroxybenzoic acid	ND	– 29.85	+	+
143	2-Hydroxy-5-[(E)-2-{4-[(*N*-methylacetamido)sulfonyl]phenyl}diazen-1-yl]benzoic acid	– 50.24	– 78.35	+	–
144	2-Hydroxy-5-[(E)-2-{4-[(thiophene-2-sulfonyl)sulfamoyl]phenyl}diazen-1-yl]benzoic acid	– 71.17	– 75.69	+	–
145	5-[(E)-2-(4-{[(1R)-3-carbamoyl-1-carboxypropyl]sulfamoyl}phenyl)diazen-1-yl]-2-hydroxybenzoic acid	NA	NA	–	NA
146	5-[(E)-2-(4-{[(2S)-2,6-diaminohexanamido]sulfonyl}phenyl)diazen-1-yl]-2-hydroxybenzoic acid	NA	NA	–	NA
147	2-Hydroxy-5-[(E)-2-{4-[(1,3-thiazole-2-sulfonyl)sulfamoyl]phenyl}diazen-1-yl]benzoic acid	NA	NA	–	NA
148	2-Hydroxy-5-[(E)-2-{4-[(2-propylpentanamido)sulfonyl]phenyl}diazen-1-yl]benzoic acid	ND	– 72.11	+	+
149	2-Hydroxy-5-[(E)-2-{4-[(2-oxopropanamido)sulfonyl]phenyl}diazen-1-yl]benzoic acid	– 46.87	– 72.11	+	–
150	5-[(E)-2-{4-[(benzenesulfonyl)sulfamoyl]phenyl}diazen-1-yl]-2-hydroxybenzoic acid	– 53.75	– 78.77	+	–

Table 2 (continued)

	IUPAC name of amides	MTB	SA	Lipinski's rule	ADMET
151	2-Hydroxy-5-[(E)-2-{4-[(*N*-phenylformamido)sulfonyl]phenyl}diazen-1-yl]benzoic acid	− 41.85	− 58.47	+	+
152	5-[(E)-2-(4-{[(4-amino-1H-imidazol-5-yl)formamido]sulfonyl}phenyl)diazen-1-yl]-2-hydroxybenzoic acid	NA	NA	−	NA
153	2-Hydroxy-5-[(E)-2-{4-[(piperidine-1-sulfonyl)sulfamoyl]phenyl}diazen-1-yl]benzoic acid	NA	NA	−	NA
154	5-[(E)-2-(4-{[*N*-(4-carboxyphenyl)acetamido]sulfonyl}phenyl)diazen-1-yl]-2-hydroxybenzoic acid	NA	NA	−	NA
155	C1 (MTB)	− 40.58	NA	+	+
156	C2 (SA)	NA	− 44.31	+	+

In the table 'ND' denotes there were no docking pose for the molecules, 'NA' denotes the molecules hadn't passed the Lipinski rule. '+' sign denotes that the amides have passed Lipinski's rule and ADMET filter, '−' denotes they haven't passe Lipinski's rule and ADMET filter

and oral bioavailability. Because all parameters can be easily computed, the RO5 (or its variants) has become the most widely useful filter in virtual library design (Lipinski 2004).

Quantum chemistry calculation

DFT (density functional theory) calculations have been performed by Gaussian 09W (Frisch et al. 2009). Gaussian calculation setup has been done in Gaussian 09 software using Becke's three-parameter exchange potential and Lee–Yang–Parr correlation functional (B3LYP) theory with basis set 6–31G (Becke 1993; Gill et al. 1992; Devlin et al. 1995). The surfaces (molecular orbital, density, potential) and electrostatic potential charges (EPS) have calculated the highest occupied molecular orbital (HOMO) and lowest unoccupied molecular orbital (LUMO) (Fukui et al. 1952). Chemical reactivity, intermolecular interactions and kinetic stability of molecules are characterized by the energy difference of HOMO–LUMO functions (Rauk 1994; Fleming 2011; Strom and Wilson 2013; Brownell et al. 2013). Interaction between the HOMO of the drug (amides) and the LUMO of the receptor (pantothenate synthetase) is the key factor of drug activity. Tight binding of drugs with the receptor can be achieved by increasing HOMO energy and decreasing LUMO energy in the drug molecule (El-Henawy et al. 2013).

Pharmacophore generation

A pharmacophore model is an ensemble of steric and electronic features that is necessary to ensure the optimal supramolecular interactions with a specific biological target and to trigger (or block) its biological response (Wermuth et al. 1998). The generated pharmacophore models based on receptor-ligand interactions have confirmed all substantial interactions in the compound-receptor interaction modes (Meduru et al. 2016). In a structure-based pharmacophore model, possible interaction area between the drug target (receptor) and ligands are examined (Böhm 1992).

The structure-based pharmacophore (SBP) method employed in Discovery Studio is a typical example of a macromolecule-based approach. SBP converts LUDI interaction maps within the protein-binding site into catalyst pharmacophoric features: H-bond acceptor, H-bond donor and hydrophobe. The computer program LUDI is a new method for the de novo design of enzyme inhibitors (Böhm 1992; Yang 2010). Its interaction maps comprise of a large number of catalyst features (Yang 2010).

In the present work, pharmacophore generation executed by receptor-ligand pharmacophore generation with Discovery Studio 4 for study the interactions between protein and ligand. The receptor-ligand pharmacophore generation produces few pharmacophore models from a receptor-ligand complex. The model is generated from the features that are related to the receptor-ligand docking interactions. The following ligand features types are considered: hydrogen bond acceptor, hydrophobic feature, ionizable feature and aromatic ring.

Drug–DNA interaction

Drugs (amides) can interact with different coordinates (groove) of DNA, creating different binding patterns (Chaires 1998). Each pattern has its own significance (Chen et al. 1993). Study and recognition of these patterns lead to fruitful estimate of binding modes and site selectivity which will be contributory for developments in the understanding of new drug molecules as potent and selective gene-regulatory drugs (Chaires 1998; Chen et al. 1993).

To find the binding pattern of Amides with MTBDNA (pdb id: 3pvp), docking method is used. Drug-DNA docking is done by autodock vina software on Windows platform with 8 Gb RAM and Intel I 5 processor (Trott and Olson 2010).

Table 3 Selected sulfonamides of higher docking score than C1 with MTB pantothenate synthetase and passed the Lipinski's rule and ADMET filter. IUPAC names (Serial No. Table 2) and CDOCKER energy (CDE). The name of the drug group are given below. Added functional groups are in coloured circle

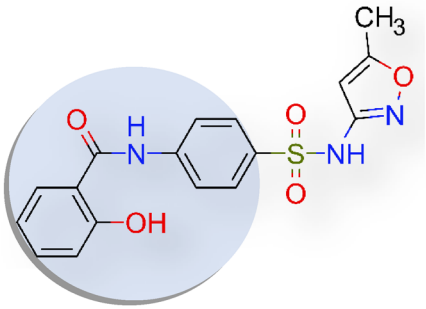 2-hydroxy-*N*-{4-[(5-methyl-1,2-oxazol-3-yl) sulfamoyl]phenyl}benzamide (No.4; CDE = - 56.43) **SULFAMETHOXAZOLE**	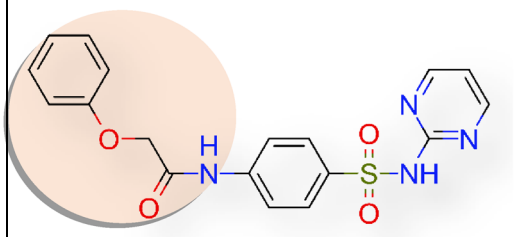 *N*-{4-[(5,6-dimethoxypyrimidin-4-yl sulfamoyl]phenyl}-*N*-phenylformamide (No.121; CDE = -41.87) **SULFADOXINE**
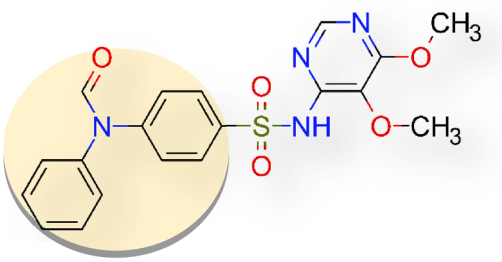 2-phenoxy-*N*-{4-[(pyrimidin-2-yl)sulfamoyl]phenyl}acetamide (No.68; CDE = -49.30) **SULFADIAZINE**	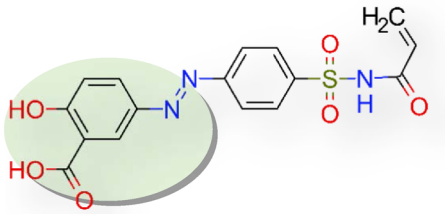 2-Hydroxy-5-[(E)-2-{4-[(prop-2-enamido)sulfonyl]phenyl}diazen-1-yl]benzoic acid **(M1)** (No.135; CDE= -66.41) **SULFASALAINE**
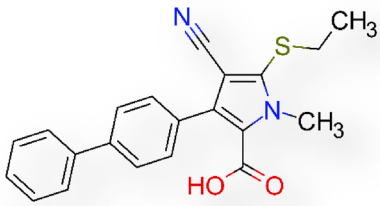 3-{[1,1'-biphenyl]-4-yl}-4-cyano-5-(ethylsulfanyl)-1-methyl-1H-pyrrole-2-carboxylic acid (Compound1) (No.155; CDE= -40.58)	

ADMET

Before a drug applies pharmacodynamics effect on the body via interaction with its target, it must transport through the body to reach the site of drug action. Pharmacokinetics denotes to the expedition of the drug from its point of entrance to the site of action. Generally speaking, this process can be defined by the following phases: absorption, distribution, metabolism, excretion and toxicity called ADMET (Roncaglioni et al. 2013). Competence of the drug to reach pharmacologically active concentration at the drug targets without any undesirable effect is taken care by ADMET properties which include the calculation of a series of factors (Lin et al. 2013).

In the present study, ADMET has been carried out by evaluating water solubility, human intestinal absorption, oral bioavailability, blood–brain barrier penetration, transporter, plasma protein binding, volume of distribution, CYP450,

Table 4 Selected sulfonamides of higher docking score than C2 with SA pantothenate synthetase and passed the Lipinski's rule and ADMET filter. IUPAC names (Serial no; Table 2) and CDOCKER energy (CDE).The name of the drug group are given below. Added functional groups are in coloured circle

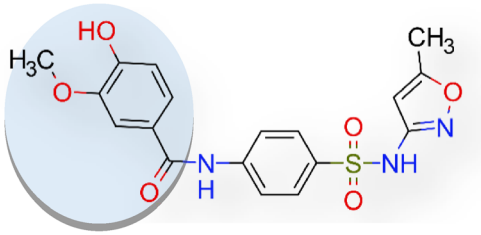 4-hydroxy-3-methoxy-*N*-{4-[(5-methyl-1,2-oxazol-3-yl)sulfamoyl]phenyl}benzamide (No.39; CDE=-70.46) **SULFAMETHOXAZOLE**	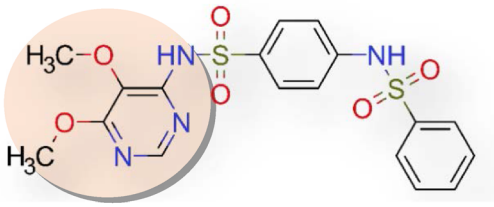 4-benzenesulfonamido-*N*-(5,6-dimethoxypyrimidin-4-yl)benzene-1-sulfonamide (No.119; CDE=-51.50) **SULFADOXINE**
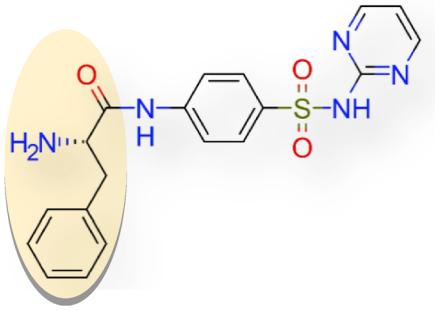 (2S)-2-amino-3-phenyl-*N*-{4-[(pyrimidin-2-yl) sulfamoyl]phenyl}propanamide (No.49, CDE=-52.08) **SULFADIAZINE**	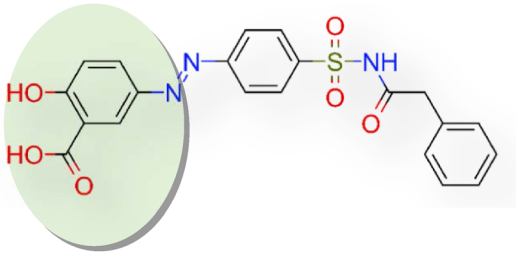 2-hydroxy-5-[(E)-2-{4-[(2-phenylacetamido)sulfonyl]phenyl}diazen-1-yl]benzoic acid **(M2)** (No.129; CDE=-**85.41**) **SULFASALAINE**
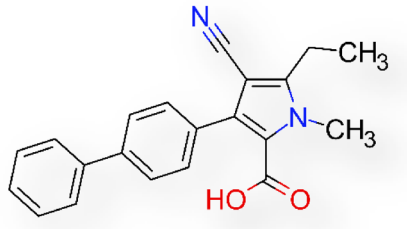 3-{[1,1'-biphenyl]-4-yl}-4-cyano-5-ethyl-1-methyl-1H-pyrrole-2-carboxylic acid (Compound 2) **(No. 156 CDE= -44.31)**	

toxicity etc. by support vector machine (SVM) algorithm (Cheng et al. 2012).

Molecular dynamics simulation

Molecular dynamics simulation (MD simulation) is calculated to confirm further the interaction strength and stability of the receptor-ligand complex determined from molecular docking by Discovery Studio's standard dynamics cascade wizard.

The same pdb file which is modified for docking and 2-hydroxy-5-[(E)-2-{4-[(prop-2-enamido) sulfonyl] phenyl} diazen-1-yl] benzoicacid are taken as protein–ligand complexes. For DNA MD simulation, same DNA is

chosen. Prior to performing MD simulations, charm force field has been applied to each of the protein–ligand complexes and solvation is set to explicit periodic boundary (Brooks et al. 1983). The parameters for MD simulations are set with following conditions: both steepest descent of energy minimization and steps of conjugate gradient minimization are done in order to obtain constant and reasonable conformation of biomolecules (Petrova and Solov'ev 1997; Hestenes and Stiefel 1952). The system was heated from an initial temperature of 50 K to the target temperature of 300 K, and the equilibration steps are done. Moreover, the parameters of electrostatics are chosen as particle mesh Ewald (PME) for long-range electrostatic constrains (Darden et al. 1993). The total production time of 53 ps simulations and are performed with NVT (dynamics without temperature/pressure control) (Beard and Qian 2010). Default setting values are adopted for other parameters.

Results and discussions

Sequence alignment analysis

The sequence alignment analysis has been carried out by Clustal Omega and the results are tabulated in Table 1. These results used to observe similarities between different pantothenate synthetase (Sievers and Higgins 2014). There is no significant match between MTB pantothenate synthetase and other pantothenate synthetase. Clustal Omega reveals that *Neisseria gonorrhoeae* pantothenate synthetase has 45.71% similarity with MTB pantothenate synthetase.

Clustal Omega with the support of percent identity matrix (PIM) shows that SA pantothenate synthetase has 45.71% similarity with Thermotoga maritima pantothenate synthetase (Chenna et al. 2003). These sequences give an idea of biological species evolution. The sequence similarity would be a motive for drug designers to work with other species containing pantothenate synthetase.

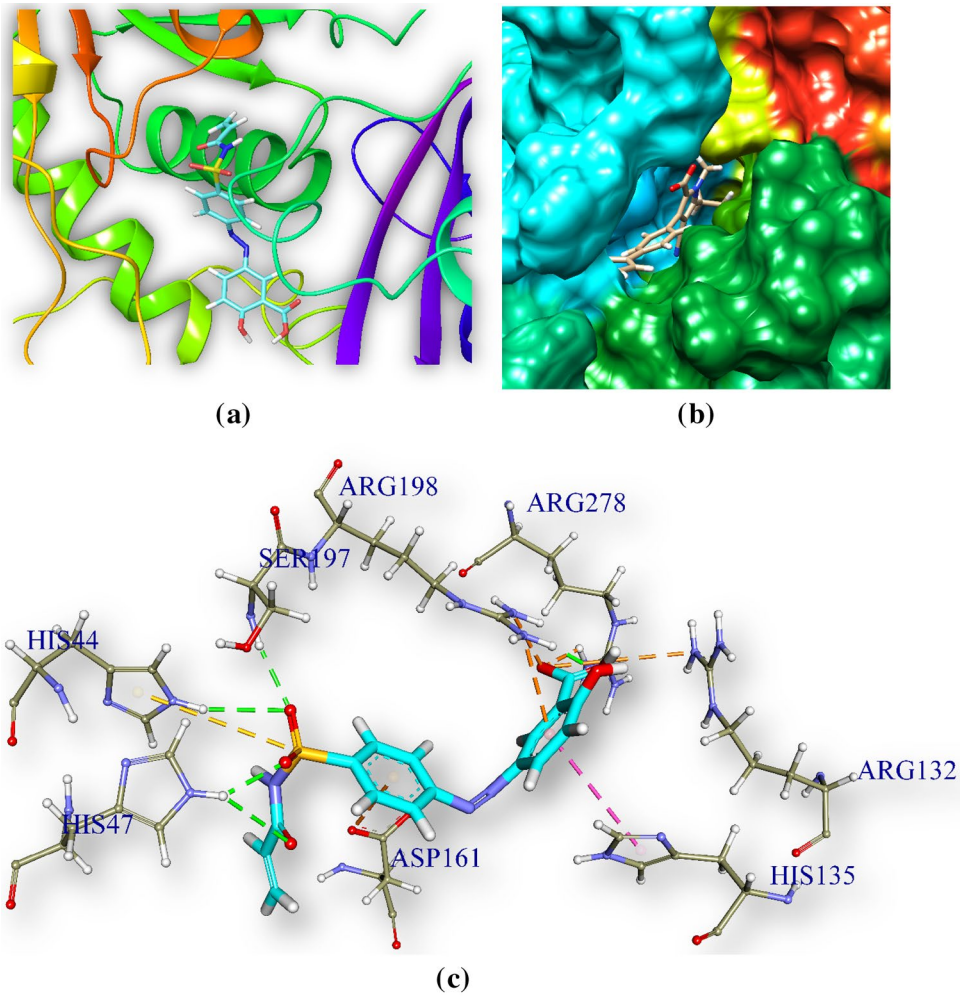

Fig. 2 Docked comprehensive perception of MTB pantothenate synthetase and **M1** after docking. **a** p.s is represented by ribbon and M1 is represented by stick and coloured according to elements. **b** secondary structure of p.s represented by hydrophobic surface and M1 represented is by stick model, **c** interactions of M1 with p.s amino acids. Bonds are in dots. M1 surrounding amino acids are in three letters code, represented in blue

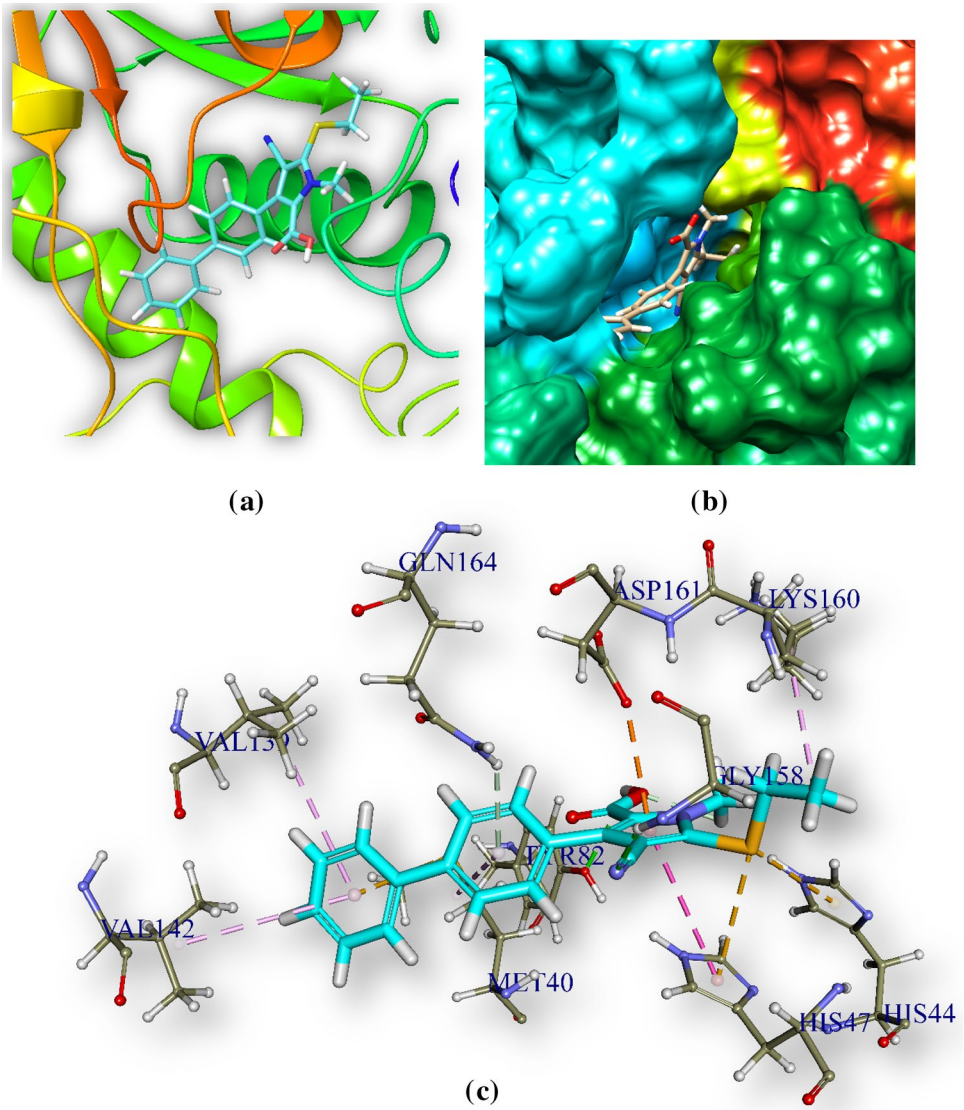

Fig. 3 Docked comprehensive perception of pantothenate synthetase and C1 interaction after docking. Picture legends representation are same as Fig. 1

Docking and bond analysis

The specific binding of a ligand (drug) to a drug target molecule is the key to drug action. Each ligand binds favorably to a specific site on the surface of the target molecule. Identification of the ligand-binding site for each specific protein molecule is crucially important when trying to find a suitable drug molecule for the target, and it is also important to understand the function of the protein (Soga et al. 2007). The docking analysis scores of 93 compounds with MTB and SA pantothenate synthetase have been recorded in Table 2. On comparing with CDOCKER energy of C1 and C2, useful tuberculosis drugs A (Table 1) and B (Table 2) show best score for MTB. The CDOCKER energy of M1 − 66.41 a.u. (MTB pantothenate synthetase) and energy of C1 is − 40.58 a.u. M2 shows best score for SA, and CDOCKER energy is − 70.69 a.u. and − 44.31 a.u. for C2.

2-Hydroxy-5-[(E)-2-{4-[(prop-2-enamido)sulfonyl]phenyl}diazen-1-yl]benzoic acid (M1) and pantothenate synthetase

M1 is docked in the active site of pantothenate synthetase of MTB. It forms 9 hydrogen bonds with amino acids of the pantothenate synthetase in the ranging distance 2.78–3.34 Å (Table 5, Fig. 2). It also forms 2 electrostatic bonds with amino acids of the ps. The hydrogen bond forming amino acids are asparagine (ARG278), arginine (ARG198), serine (SER197 and SER19), tyrosine (TYR82). The CDOCKER energy is − 66.41 a.u. and CDOCKER energy is − 39.54.

C1 and pantothenate synthetase

C1 (Table 1) is docked in the active site of pantothenate synthetase of MTB. It forms three hydrogen bonds with amino acids of the pantothenate synthetase within the ranging distance of 2.23–3.09 Å (Table 5, Fig. 3).The hydrogen

bond forming amino acids are Glycine (GLY158), Tyrosine TYR82, Glycine GLN164, Aspartate ASP161. The CDOCKER energy is − 40.58 a.u. and CDOCKER energy is − 5.52 a.u (Fig. 3).

5-[(E)-2-{4-[(4-aminobenzenesulfonyl) sulfamoyl] phenyl} diazen-1-yl]-2-hydroxybenzoic acid (M2) and *Staphylococcus aureus* pantothenate synthetase

M2 is docked in the active site of *Staphylococcus aureus* pantothenate synthetase. It forms twelve hydrogen bonds ranging between 1.67 and 3.08 Å (Table 6, Fig. 4). It also forms an electrostatic interaction at a distance of 3.60 Å. The hydrogen bond forming amino acids are serine (SER186), glutamine (GLN154), lysine (LYS150), arginine (ARG188) histidine (HIS38), methionine (MET31) and threonine (THR30). The CDOCKER energy is − 85.41 a. u. followed by CDOCKER energy is 57.64 a.u. It also forms 1 electrostatic bonds with amino acids of the ps

C2 and pantothenate synthetase

C2 is docked in the active site of SA pantothenate synthetase. It forms three hydrogen bonds with amino acids of the pantothenate synthetase within the ranging distance of 1.9–3.9 Å (Table 6, Fig. 5).The hydrogen bond forming amino acids are Arginine (ARG122,ARG188, ARG273), Histidine (HIS38), Lysine(LYS150), Threonine (THR30), Methionine(MET31). It also forms 1 electrostatic bonds with amino acids of the ps. The CDOCKER energy is − 44.31 a.u and CDOCKER energy is − 9.07 a.u.

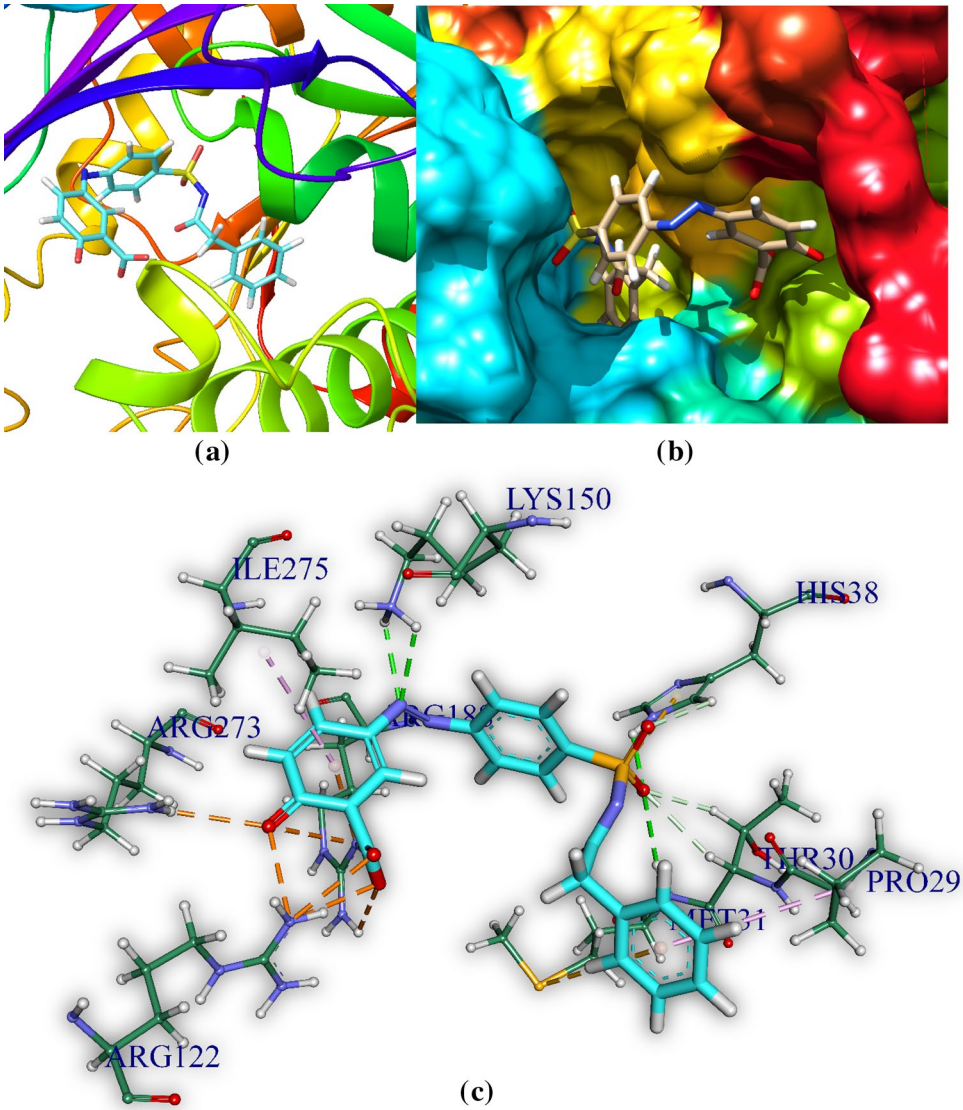

Fig. 4 Docked comprehensive perception *M2* and *Staphylococcus aureus* pantothenate synthetase after docking. Picture legends representation is same as Fig. 2

Table 5 Noncovalent bond distances between 2-hydroxy-5-[(E)-2-{4-[(prop-2-enamido) sulfonyl] phenyl} diazen-1-yl] benzoic acid, C1 and pantothenate synthetase

Noncovalent bond distances between M1 (Lig1) (Table 1) and MTB ps	Distance (Å)	Bonding category	Noncovalent bond distances between C1 (Lig2) and MTB pantothenate synthetase	Distance (Å)	Bonding category
A:ARG198:NH2—Lig1:O26	2.70	Electrostatic	A:GLY158:HN—Lig2:N21	2.23	Hydrogen bond
A:ARG278:NH1—Lig1:O9	2.78	Hydrogen bond	Lig2:H44—A:TYR82:OH	3.043	Hydrogen bond
A:ARG198:NH1—Lig1:O9	2.83	Hydrogen bond	A:GLN164:HE22—Lig2	3.09	Hydrogen bond
A:ARG278:NH1—Lig1:O8	2.87	Electrostatic	A:ASP161:OD2—Lig2	3.53	Electrostatic
A:SER197:OG—Lig1:O23	3.20	Hydrogen bond			
A:SER197:N—Lig1:O23	3.28	Hydrogen bond			
A:TYR82:OH—Lig1:O25	3.34	Hydrogen bond			
A:ARG198:NH2—Lig1	3.52	Hydrogen bond			
A:ASP161:OD2—Lig1	3.53	Hydrogen bond			
A:ARG132:NH2—Lig1:O8	3.60	Hydrogen bond			
A:ARG198:NH1—Lig1:O8	3.81	Hydrogen bond			

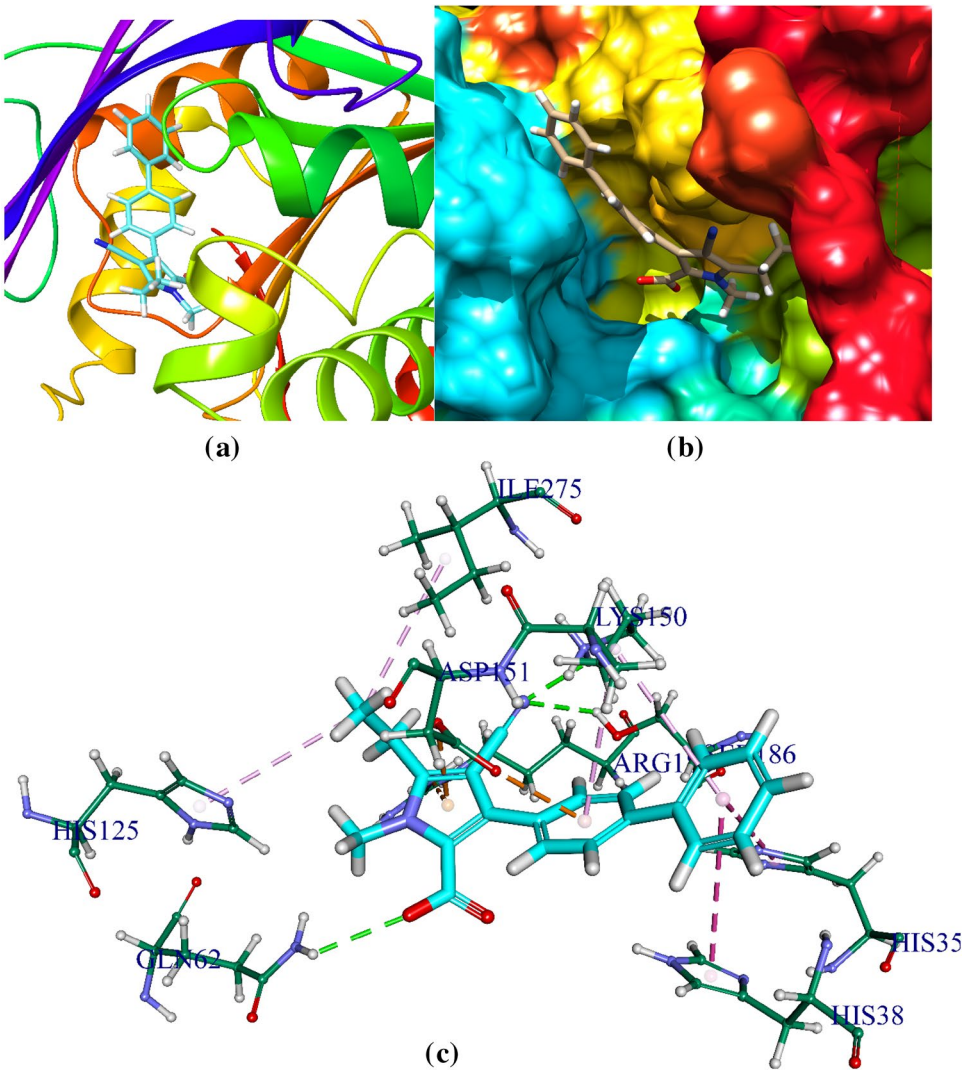

Fig. 5 Comprehensive perception of C2 and *Staphylococcus aureus* pantothenate synthetase interaction after docking. Picture legends representation are same as Fig. 2

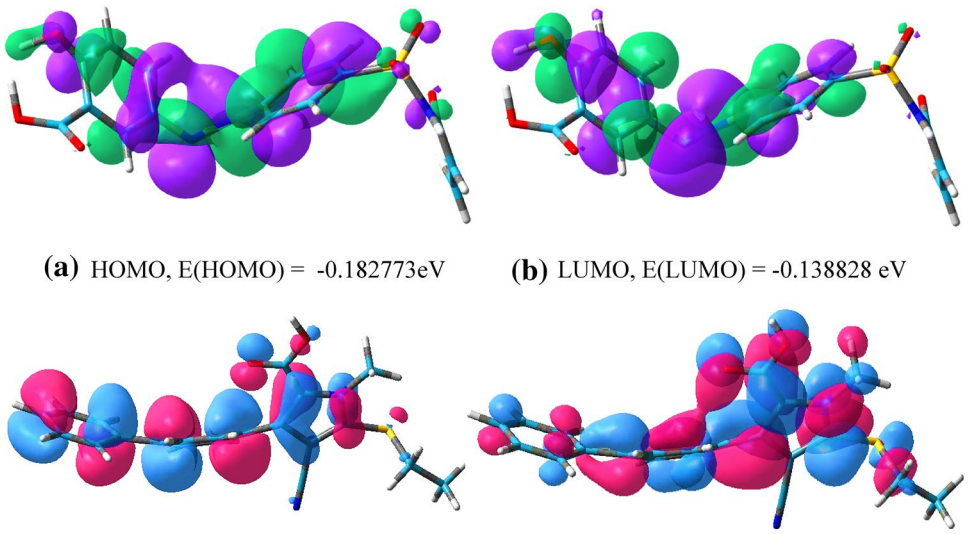

Fig. 6 **a**, **b** HOMO and LUMO plots of *M1*. The positive electron density has been shown in green color while negative in violet. **c**, **d** HOMO and LUMO plots of C1. The positive electron density has been shown in red color while negative in blue

ADMET property analysis

There are total 26 parameters in ADMET data which were available in literature (Cheng et al. 2012). In the present work a '+' sign is marked when 23 parameters are positive (81%) and '++' is assigned (Table 7) when more than 23 parameters are passed (Cheng et al. 2012). Pharmacokinetic properties and toxicities are predicted by ADMET which can predict permeability for BBB (blood–brain barrier), HIA (human intestinal absorption), P-glycoprotein substrate/inhibitor, renal organic cation transporter, etc. ADMET result shows 2-hydroxy-5-[(E)-2-{4-[(prop-2-enamido)sulfonyl]phenyl}diazen-1-yl]benzoic acid and 2-hydroxy-5-[(E)-2-{4-[(2-phenylacetamido)sulfonyl]phenyl}diazen-1-yl]benzoic acid are positive (+) in HIA, BBB permeability. It suggests that the molecules are well absorbed in human

Table 6 Recognizable bonds between ***M2***, C2 and *Staphylococcus aureus* Pantothenate synthetase

Noncovalent bond distances bonds between ***M2*** (LIG3) and SA pantothenate synthetase	Distance (Å)	Bonding category	Noncovalent bond distances between C2 (Lig4) and SA ps	Distance (Å)	Category
A: LYS150:HZ3 - :LIG3: O	1.67	Hydrogen bond; Electrostatic	A:ARG188:HH22—:LIG4:O	1.9	Hydrogen bond; Electrostatic
A: SER186: HG - :LIG3: O	1.91	Hydrogen bond	A:HIS38:HE2 - :LIG4:O	2.11	Hydrogen bond
A: GLN154:HE22 - :LIG3: O	1.93	Hydrogen bond	A:LYS150:HZ3 - :LIG4:N	2.43	Hydrogen bond
A: LYS150:HZ2 - :LIG3: O	2.15	Hydrogen bond; Electrostatic	A:LYS150:HZ2 - :LIG4:N	2.63	Hydrogen bond
A:ARG188:HH22 - :LIG3:N	2.26	Hydrogen bond	A:THR30:HA - :LIG4:O	2.72	Hydrogen bond
A: HIS38:HE2 - :LIG3: O	2.38	Hydrogen bond	A:ARG273:HH11 - :LIG4:O	2.75	Hydrogen bond; Electrostatic
A: MET31: HN - :LIG3: O	2.45	Hydrogen bond	A:MET31:HN - :LIG4:O	2.77	Hydrogen bond
A: THR30: HA - :LIG3: O	2.51	Hydrogen bond	A:THR30:HB - :LIG4:O	2.78	Hydrogen bond
A: SER186:HB2 - :LIG3: O	2.68	Hydrogen bond	A:ARG122:NH2 - :LIG4:O	2.83	Electrostatic
A: LYS150:HE1 - :LIG3: O	2.69	Hydrogen bond	A:HIS38:HD2 - :LIG4:O	2.94	Hydrogen bond
A: SER186:HB2 - :LIG3: O	2.81	Hydrogen bond	A:ARG122:NH2 - :LIG4:O	2.95	Electrostatic
A: SER186: HA - :LIG3: O	3.08	Hydrogen bond	A:ARG122:NH2 - :LIG4:O	3.00	Electrostatic
A:ARG188:NH2 - :LIG3	3.60	Electrostatic	A:ARG188:NH2 - :LIG4	3.19	Electrostatic
			A:ARG188:HH11 - :LIG4:O	3.20	Hydrogen bond; Electrostatic
			A:ARG188:NH2 - :LIG4:O	3.90	Electrostatic

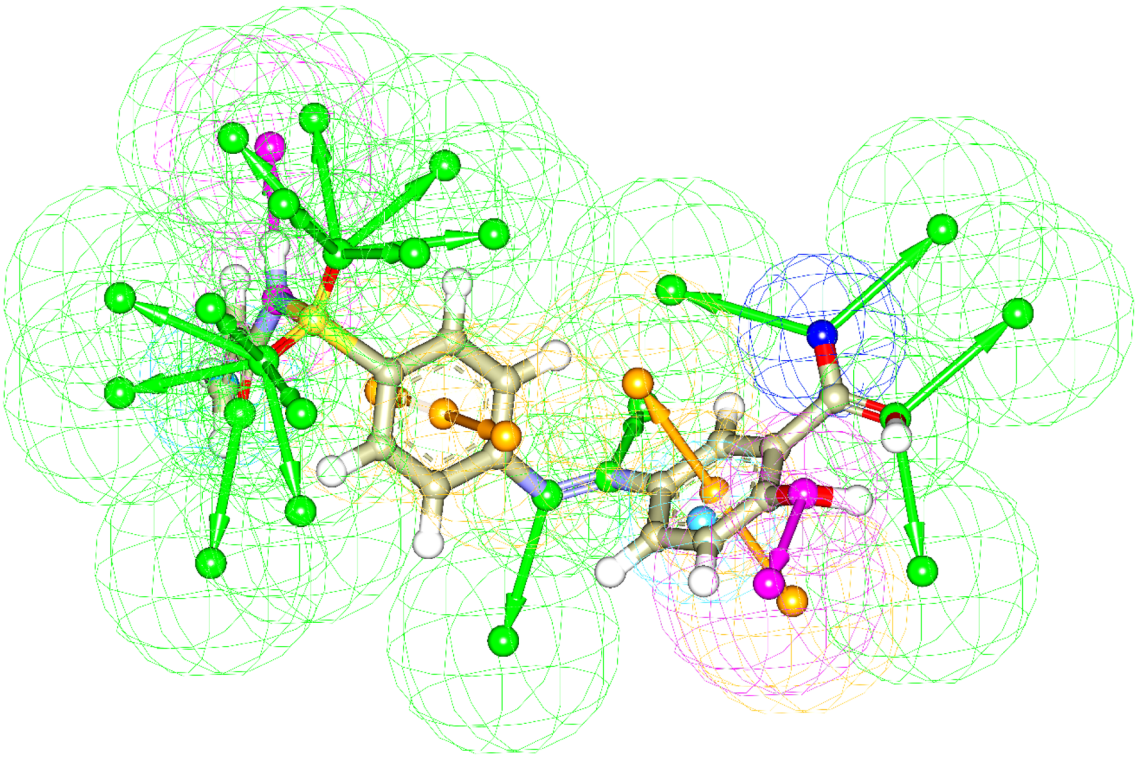

Fig. 7 The result of pharmacophore features of *M1* based on receptor-ligand pharmacophore generation. The hydrogen bond acceptor, hydrogen bond donor, positive ionizablefeature, aromatic ring and negative ionizable features are shown as green, orange and blue respectively

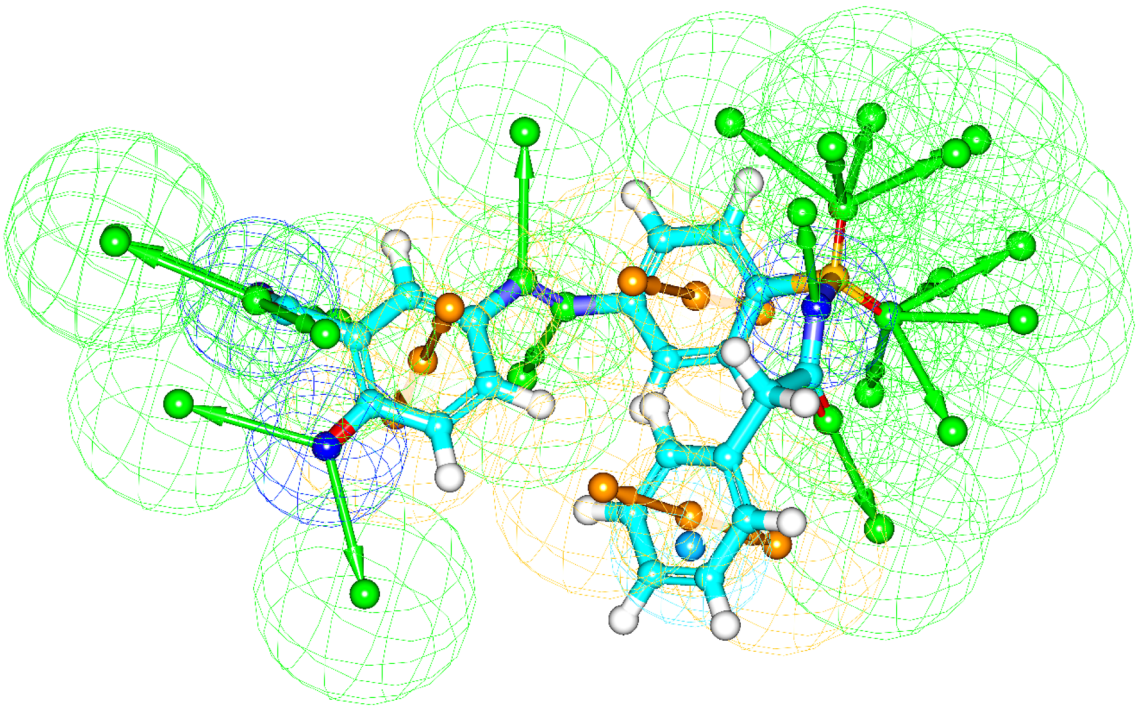

Fig. 8 The result of pharmacophore features of *M2* based on receptor-ligand pharmacophore generation. The hydrogen bond acceptor, hydrogen bond donor, positive ionizablefeature, aromatic ring and negative ionizable features are shown as green, orange, and blue respectively

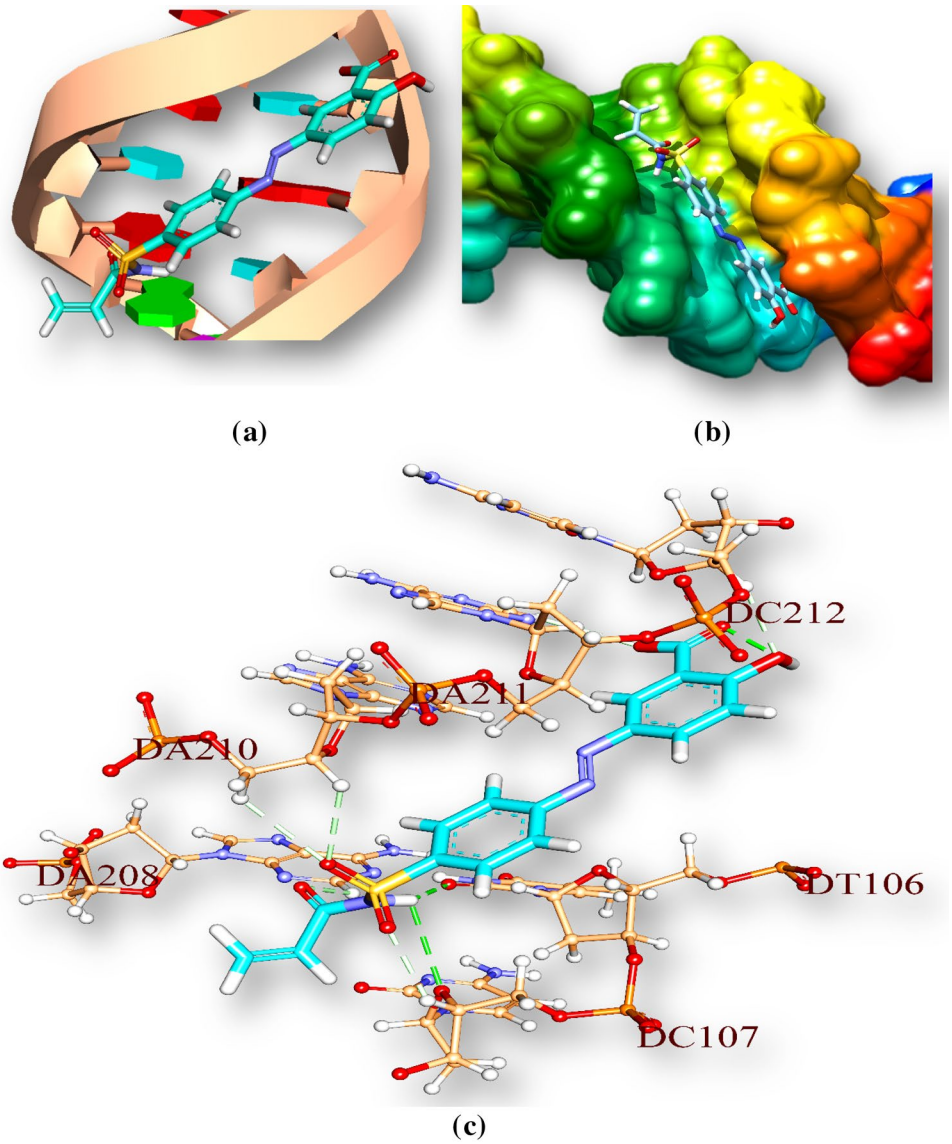

Fig. 9 **M1** interaction with Tuberculosis's DNA in minor groove. **a** Drug is represented by stick and double helical DNA structure is represented by ladder and rings, **b** double helical structure of DNA represented by ***M1*** represented by stick model and are coloured according to elements, **c** interactions of ligand with DNA base pairs (A, T, G, C); the interaction types. Hydrogen bonds are in green. Ligand surrounding base pairs are in three letters code represented in black

body (Table 7). Inhibition and initiation of P-glycoprotein have been reported as the causes of drug–drug interactions (Lin and Yamazaki 2003). Two best docked molecules (M1 and M2) are P-glycoprotein non-inhibitor. Data in Table 8 show the best fitted ligand in permissible limit (Lin et al. 2013). Organiccation transporters are responsible for drug absorption and disposition in the kidney, liver, and intestine (Zhang et al. 1998). ADMET result of two best docked molecules shows that they are non-inhibitor of renal organic cation transporter. The human cytochromes P450 (CYPs), particularly isoforms 1A2, 2C9, 2D6 and 3A4 are responsible for about 90% oxidative metabolic reactions. Inhibition of CYP enzymes will lead to inductive or inhibitory failure of drug metabolism (Uttamsingh et al. 2005).

The Ames test is a widely employed method that uses bacteria to test whether a given chemical can cause cancer. More formally, it is a biological assay to assess the mutagenic potential of chemical compounds (Ames et al. 1972; Mortelmans and Zeiger 2000).

Human Ether-à-go–go-Related Gene (hERG) is a gene sensitive to drug binding (Sanguinetti and Tristani-Firouzi 2006). ADMET results show that the drugs M1, M2 are weak inhibitor and non-inhibitor of hERG (predictor I and II) (Sanguinetti and Tristani-Firouzi 2006). The aqueous solubility (logS) of a compound considerably affects its absorption and distribution properties. The predicted logS values of the studied compounds are within the acceptable limit (Vyas et al. 2013). The solubility (logS) of organic molecules in water is considered in the ADMET, because this parameter generally has important impact on many ADMET concerned properties of drugs, such as uptake, distribution, transport and eventually bioavailability (Hou

Table 7 ADMET properties of M1 and C1

ADMET properties	M1		C1	
	Value	Probability	Value	Probability
Absorption				
Blood–brain barrier	+	0.6541	+	0.8722
Human intestinal absorption	+	0.8131	+	0.9727
Caco-2 permeability	–	0.6518	+	0.5769
P-glycoprotein substrate	Non-substrate	0.8458	Non-substrate	0.8551
P-glycoprotein inhibitor	Non-inhibitor	0.8955	Non-inhibitor	0.8246
	Non-inhibitor	0.8994	Inhibitor	0.7104
Renal organic cation transporter	Non-inhibitor	0.9100	Non-inhibitor	0.7486
Distribution				
Subcellular localization	Mitochondria	0.5965	Mitochondria	0.7434
Metabolism				
CYP450 2C9 substrate	Non-substrate	0.5802	Non-substrate	0.6852
CYP450 2D6 substrate	Non-substrate	0.8518	Non-substrate	0.8225
CYP450 3A4 substrate	Non-substrate	0.6784	Non-substrate	0.6153
CYP450 1A2 inhibitor	Non-inhibitor	0.8434	Non-inhibitor	0.5117
CYP450 2C9 inhibitor	Inhibitor	0.8248	Inhibitor	0.6145
CYP450 2D6 inhibitor	Non-inhibitor	0.8765	Non-inhibitor	0.8789
CYP450 2C19 inhibitor	Non-inhibitor	0.7830	Inhibitor	0.5904
CYP450 3A4 inhibitor	Non-inhibitor	0.7587	Non-inhibitor	0.8283
CYP inhibitory promiscuity	Low CYP inhibitory promiscuity	0.7264	High CYP inhibitory promiscuity	0.8456
Toxicity				
Human Ether-a-go–go-related gene inhibition	Weak inhibitor	0.9825	Weak inhibitor	0.9972
	Non-inhibitor	0.8904	Non-inhibitor	0.7206
AMES toxicity	Non AMES toxic	0.7342	Non AMES toxic	0.7595
Carcinogens	Non-carcinogens	0.5385	Non-carcinogens	0.8117
Fish toxicity	High FHMT	0.9977	High FHMT	0.9710
Tetrahymena pyriformis toxicity	High TPT	0.8832	High TPT	0.8240
Honey bee toxicity	Low HBT	0.7391	Low HBT	0.7051
Biodegradation	Not ready biodegradable	0.9836	Not ready biodegradable	0.9936
Acute oral toxicity	III	0.6643	III	0.4468
Carcinogenicity (three-class)	Non-required	0.5722	Non-required	0.5471

et al. 2004). Understanding of ADMET properties together with their measurement and prediction gives an idea about the dose size and dose frequency, drugs solubility, metabolism of drug and its toxicity. Before synthesizing drug like molecules in laboratory, a profound knowledge of drug properties will save time and resources.

Density functional theory analysis

HSFs from the best binding pose have been transferred to Gauss view 5 and the difference in HOMO and LUMO energy, known as band gap, indicates the electronic excitation energy, necessary to compute the molecular reactivity and stability of the compounds (Becke 1993; Gill et al. 1992; Devlin et al. 1995; Fukui et al. 1952). For 2-hydroxy-5-[(E)-2-{4-[(prop-2-enamido)sulfonyl]phenyl} diazen-1-yl] benzoic acid, eigen values of HOMO and LUMO are − 0.182773 and − 0.138828 eV respectively and the HOMO–LUMO gap is − 0.043945. For compound 1, eigen values of HOMO and LUMO are − 0.213889 and − 0.053971 eV and the HOMO–LUMO gap is − 0.159918 eV (Figs. 5, 6; Table 6).

Pharmacophore generation

The generated pharmacophore models based on receptor-ligand interactions by docking have confirmed all major interactions in the drug-receptor interaction modes. The number of features, feature set and selectivity score from

Table 8 ADMET properties of M2 and C2

ADMET properties	M2		C2	
	Value	Probability	Value	Probability
Absorption				
Blood–brain barrier	+	0.6917	+	0.8646
Human intestinal absorption	+	0.7727	+	0.9974
Caco-2 permeability	–	0.7290	+	0.6995
P-glycoprotein Substrate	Non-substrate	0.8093	Non-substrate	0.7334
P-glycoprotein Inhibitor	Non-inhibitor	0.9111	Non-inhibitor	0.8353
	Non-inhibitor	0.8988	Non-inhibitor	0.6629
Renal organic cation transporter	Non-inhibitor	0.8985	Non-inhibitor	0.7101
Distribution				
Subcellular localization	Mitochondria	0.5996	Mitochondria	0.7147
Metabolism				
CYP450 2C9 Substrate	Non-substrate	0.5626	Non-substrate	0.6468
CYP450 2D6 substrate	Non-substrate	0.8561	Non-substrate	0.8068
CYP450 3A4 substrate	Non-substrate	0.6266	Non-substrate	0.5928
CYP450 1A2 inhibitor	Non-inhibitor	0.8540	Non-inhibitor	0.6955
CYP450 2C9 inhibitor	Inhibitor	0.7520	Inhibitor	0.5256
CYP450 2D6 inhibitor	Non-inhibitor	0.8908	Non-inhibitor	0.9153
CYP450 2C19 inhibitor	Non-inhibitor	0.7418	Non-inhibitor	0.6502
CYP450 3A4 inhibitor	Non-inhibitor	0.8894	Non-inhibitor	0.7977
CYP inhibitory promiscuity	Low CYP inhibitory promiscuity	0.5715	High CYP inhibitory promiscuity	0.7357
Toxicity				
Human Ether-a-go–go-related gene inhibition	Weak inhibitor	0.9740	Weak inhibitor	0.9905
	Non-inhibitor	0.8964	Non-inhibitor	0.8962
AMES toxicity	Non AMES toxic	0.7293	Non AMES toxic	0.8398
Carcinogens	Non-carcinogens	0.5519	Non-carcinogens	0.8317
Fish toxicity	High FHMT	0.9604	High FHMT	0.9634
Tetrahymena pyriformis toxicity	High TPT	0.6599	High TPT	0.8293
Honey bee toxicity	Low HBT	0.7513	Low HBT	0.8206
Biodegradation	Not ready biodegradable	0.9449	Not ready biodegradable	0.9806
Acute oral toxicity	III	0.6801	II	0.6630
Carcinogenicity (three-class)	Non-required	0.5950	Non-required	0.6214

Table 9 Noncovalent bond distances between M1 and DNA (A and B chain)

Bonds	Distance (Å)	Category	Type
M1:H2 - :M1:O	2.30036	Hydrogen bond	Conventional hydrogen bond
M1:H9 - A:DT106:O2	2.36896	Hydrogen bond	Conventional hydrogen bond
M1:H9 - A:DC107:O4′	3.0371	Hydrogen bond	Conventional hydrogen bond
A:DC107:H4′ - :M1:O	2.57249	Hydrogen bond	Carbon hydrogen bond
B:DA208:H2 - :M1:O	2.50191	Hydrogen bond	Carbon hydrogen bond
B:DA210:H5′2 - :M1:O	2.91783	Hydrogen bond	Carbon hydrogen bond
B:DA210:H4′ - :M1:O	2.95761	Hydrogen bond	Carbon hydrogen bond
B:DA211:H2 - :M1:O	2.69911	Hydrogen bond	Carbon hydrogen bond
B:DC212:H4′ - :M1:O	2.54721	Hydrogen bond	Carbon hydrogen bond

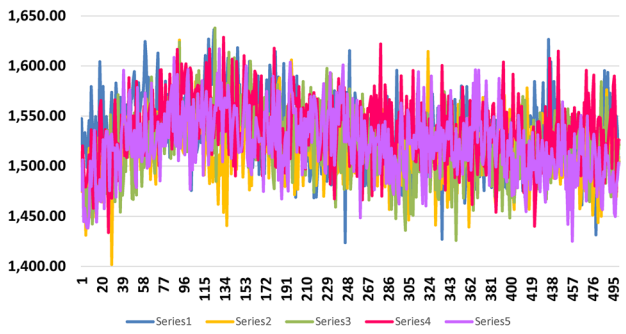

Fig. 10 Shows bond energy graph of *M1*, other four molecules of Table 3 and C1 with pantothenate synthetase of *Mycobacterium tuberculosis*. Bond energy and number of trajectory frames are plotted along X- and Y-axis respectively. Best docked molecule is in blue and C1 is in pink. (Series numbers are maintained as in Table 3)

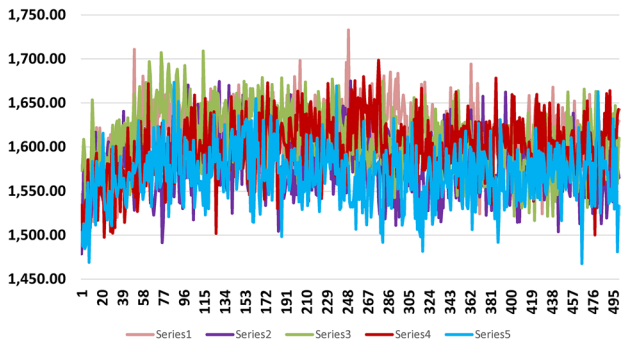

Fig. 11 Shows bond energy graph of *M2* with pantothenate synthetase of *S. aurues*. X axis and Y-axis represent the bond energy and number of trajectory frames respectively. Best docked molecule is in pink and C2 is in blue. (Series numbers are maintained as in Table 4)

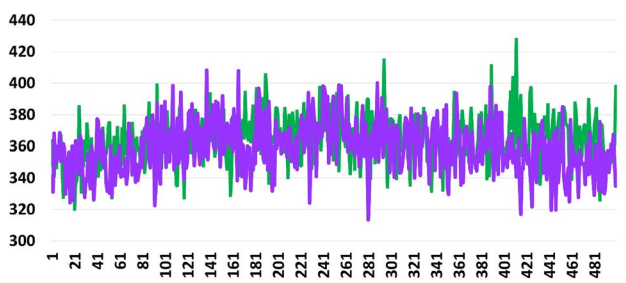

Fig. 12 Shows bond energy graph of 2-hydroxy-5-[(E)-2-{4-[(prop-2-enamido) sulfonyl] phenyl} diazen-1-yl] benzoic acid and C1 with DNA of *Mycobacterium tuberculosis*. X-axis and Y-axis represent bond energy and number of trajectory frames respectively. Best docked molecule is in green and C1 is in violet

pharmacophore generation are observed from the two best docked molecules. Pharmacophore generation of 2-Hydroxy-5-[(E)-2-{4-[(prop-2-enamido) sulfonyl]phenyl} diazen-1-yl]benzoic acid (M1) and

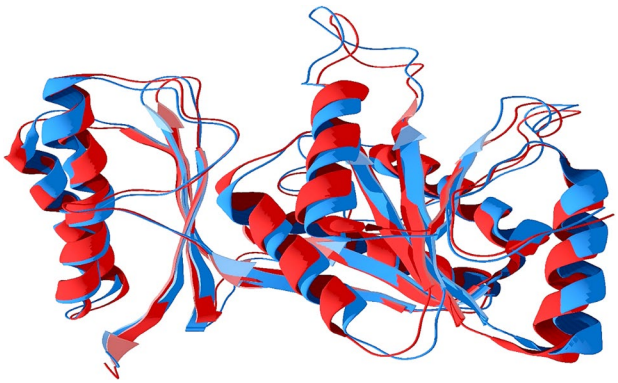

Fig. 13 Shows results of molecular dynamics, last conformation (structure) superimposed (red) with first conformation (blue) of pantothenate synthetase of *Mycobacterium tuberculosis*

2-hydroxy-5-[(E)-2-{4-[(2-phenylacetamido)sulfonyl] phenyl}diazen-1-yl]benzoic acid (M2) are shown in Figs. 7 and 8, respectively.

Drug–DNA interaction

The drug (amides)–DNA interactions have been computationally examined by docking techniques used to study interactions between DNA and small ligand molecules those are potentially pharmaceutical interest. Autodock vina software is used for docking (Trott and Olson 2010). Drug-DNA interaction gives an idea about binding pattern of drug with DNA. Amides compounds (drug) docked with *M. tuberculosis's* DNA is used to understand the drug-DNA interaction. We have observed that amide compounds interact with AT-rich regions (represented by red and turquoise coloured rings respectively) of DNA in the minor groove by forming hydrogen bonding and hydrophobic interactions (Fig. 9). The amino group of guanine (represented by green ring) prevents 2-hydroxy-5-[(E)-2-{4-[(prop-2-enamido) sulfonyl] phenyl} diazen-1-yl] benzoic acid from binding to the G·C base pairs by steric hindrance (Table 9), and thus conferring AT-selectivity on the drug molecule. Minor groove binding molecules are usually constructed of a series of heterocyclic or aromatic hydrocarbon rings that possess rotational freedom. This allows these molecules to fit into the minor groove, with displacement of water; these drugs can form hydrogen bonds to bases (Sangeetha Gowda et al. 2014).

Molecular dynamics simulation

The MD simulation study of best docked molecules with Mtb and *S. aureus* pantothenate synthetase and Mtb DNA are carried out for 53 ps by 50 thousand steps. MD production run and the trajectory of the various energy profiles are created and analyzed.

Potential energy of ***M1*** after MD simulation was − 14,633 kcal/mol and C1 − 14,607.2 kcal/mol and bond energy was 1526.3 and 1503.13 kcal/mol respectively. Same for S. aureus pantothenate ***M2*** − 16,245.9 kcal/mol bond energy was 1642.68 and 1533.34 kcal/mol respectively.

For Mtb DNA and 2-hydroxy-5-[(E)-2-{4-[(prop-2-enamido) sulfonyl]phenyl} diazen-1-yl] benzoic acid potential energy was − 2394.2 kcal/mol and bond energy was 398.096 kcal/mol. For C1 potential energy was − 2357.67 kcal/mol bond energy 334.856 kcal/mol. Bond energy graphs are shown in Figs. 10, 11 and 12.

As the graphs revealed that in all situations for the best docked molecules, the bond strength are increased from initial position, ended from the starting point of bond strength and it was higher till then end compared to corresponding drugs. So it can be clearly predicted that molecules formed stable conformation with Mtb and *S. aureus* pantothenate synthetase and DNA. Super imposed structures of first conformation (trajectory frame) and last conformation of Mtb pantothenate synthetase show the deviation of end point of the dynamics from the initial point of dynamics (Fig. 13).

Conclusion

Amide functionalized sulfa drugs show potent anti-microbial activity and also active against MTB and *S. aureus* in vivo. The best docked compounds have better docking score than approved drugs and also show better ADMET efficiency.

Out of 154 compounds, 2-hydroxy-5-[(E)-2-{4-[(prop-2-enamido)sulfonyl]phenyl}diazen-1-yl] benzoic acid and 2-hydroxy-5-[(E)-2-{4-[(2-phenylacetamido)sulfonyl]phenyl}diazen-1-yl] benzoic acid exhibit significantly higher docking score than approved drugs, C1 and C2. Molecular orbital, pharmacophore, drug likeness and ADMET predicted the idea about electrostatic pharmacological and non-toxic properties. Molecular dynamics simulation enriches the knowledge of stability of drug like molecule. We hope, will open new avenues to amide drug research. This computational prediction about a better tuberculosis drug will encourage and assist experimentalists to a great extent to design and synthesize potential new drugs for removal of this epidemic disease, spreading globally with a rapid span.

References

Ames BN, Gurney EG, Miller JA, Bartsch H (1972) Carcinogens as frameshift mutagens: metabolites and derivatives of 2-acetylaminofluorene and other aromatic amine carcinogens. Proc Natl Acad Sci USA 69(11):3128–3132

Bartzatt R, Cirillo SL, Cirillo JD (2010) Sulfonamide agents for treatment of *Staphylococcus* MRSA and MSSA infections of the central nervous system. Cent Nerv Syst Agents Med Chem 10(1):84–90

Beard DA, Qian H (2010) Chemical biophysics: quantitative analysis of cellular systems. Cambridge University Press, Cambridge

Becke AD (1993) Density-functional thermochemistry. The role of exact exchange. J Chem Phys 98(7):5648–5652

Berg JM, Tymoczko JL, Stryer L (2002) Biochemistry, 5th edn. W. H. Freeman, New York

Böhm H-J (1992) The computer program LUDI: a new method for the de novo design of enzyme inhibitors. J Comput Aided Mol Des 6(1):61–78

Brooks BR, Bruccoleri RE, Olafson BD, States DJ, Swaminathan S, Karplus M (1983) CHARMM: a program for macromolecular energy, minimization, and dynamics calculations. J Comput Chem 4(2):187–217

Brownell LV, Robins KA, Jeong Y, Lee Y, Lee D-C (2013) Highly systematic and efficient HOMO–LUMO energy gap control of thiophene-pyrazine-acenes. J Phys Chem C 117(48):25236–25247

Chaffey N, Alberts B, Johnson A, Lewis J, Raff M, Roberts K, Walter P (2003) Molecular biology of the cell, 4th edn. Ann Bot 91(3):401

Chaires JB (1998) Drug–DNA interactions. Curr Opin Struct Biol 8(3):314–320

Chen AY, Yu C, Gatto B, Liu LF (1993) DNA minor groove-binding ligands: a different class of mammalian DNA topoisomerase I inhibitors. Proc Natl Acad Sci USA 90(17):8131–8135

Cheng F, Li W, Zhou Y, Shen J, Wu Z, Liu G, Lee PW, Tang Y (2012) admetSAR: a comprehensive source and free tool for assessment of chemical ADMET properties. J Chem Inf Model 52(11):3099–3105

Chenna R, Sugawara H, Koike T, Lopez R, Gibson TJ, Higgins DG, Thompson JD (2003) Multiple sequence alignment with the clustal series of programs. Nucl Acid Res 31(13):3497–3500

Cole ST, Brosch R, Parkhill J, Garnier T, Churcher C, Harris D, Gordon SV, Eiglmeier K, Gas S, Barry CE 3rd, Tekaia F, Badcock K, Basham D, Brown D, Chillingworth T, Connor R, Davies R, Devlin K, Feltwell T, Gentles S, Hamlin N, Holroyd S, Hornsby T, Jagels K, Krogh A, McLean J, Moule S, Murphy L, Oliver K, Osborne J, Quail MA, Rajandream MA, Rogers J, Rutter S, Seeger K, Skelton J, Squares R, Squares S, Sulston JE, Taylor K, Whitehead S, Barrell BG (1998) Deciphering the biology of *Mycobacterium tuberculosis* from the complete genome sequence. Nature 393(6685):537–544

Darden T, York D, Pedersen L (1993) Particle mesh Ewald: an N·log(N) method for Ewald sums in large systems. J Chem Phys 98(12):10089–10092

Database Resources of the National Center for Biotechnology Information (2013) Nucl Acids Res 41(Database issue):D8–D20

Devlin FJ, Finley JW, Stephens PJ, Frisch MJ (1995) Ab initio calculation of vibrational absorption and circular dichroism spectra using density functional force fields: a comparison of local, nonlocal, and hybrid density functionals. J Phys Chem 99(46):16883–16902

El-Henawy AA, Khowdiary MM, Badawi AB, Soliman HM (2013) In vivo anti-leukemia, quantum chemical calculations and ADMET investigations of some quaternary and isothiouronium surfactants. Pharmaceuticals 6(5):634–649

Fleming I (2011) Molecular orbitals and organic chemical reactions, Reference edn. Wiley, Amsterdam

Frisch M, Trucks G, Schlegel H, Scuseria G, Robb M, Cheeseman J, Scalmani G, Barone V, Mennucci B, Petersson G (2009) Gaussian 09. Gaussian. Inc, Wallingford

Fukui K, Yonezawa T, Shingu H (1952) A molecular orbital theory of reactivity in aromatic hydrocarbons. J Chem Phys 20(4):722–725

Gill PMW, Johnson BG, Pople JA, Frisch MJ (1992) The performance of the Becke–Lee–Yang–Parr (B–LYP) density functional theory with various basis sets. Chem Phys Lett 197(4):499–505

Grassl SM (1992) Human placental brush-border membrane Na(+)-pantothenate cotransport. J Biol Chem 267(32):22902–22906
Hestenes MR, Stiefel E (1952) Methods of conjugate gradients for solving linear systems, vol 49
Holloway KA, Rosella L, Henry D (2016) The impact of WHO essential medicines policies on inappropriate use of antibiotics. PLoS One 11(3):e0152020
Hou T, Wang J (2008) Structure – ADME relationship: still a long way to go? Exp Opin Drug Metab Toxicol 4(6):759–770
Hou TJ, Xia K, Zhang W, Xu XJ (2004) ADME evaluation in drug discovery. 4. Prediction of aqueous solubility based on atom contribution approach. J Chem Inf Comput Sci 44(1):266–275
Jagessar RC, Rampersaud D (2007) Amides as antimicrobial agents. Life Sci J 4(4):46–49
Kumar A, Casey A, Odingo J, Kesicki EA, Abrahams G, Vieth M, Masquelin T, Mizrahi V, Hipskind PA, Sherman DR, Parish T (2013) A high-throughput screen against pantothenate synthetase (PanC) identifies 3-biphenyl-4-cyanopyrrole-2-carboxylic acids as a new class of inhibitor with activity against *Mycobacterium tuberculosis*. PLoS One 8(11):e72786
Leonardi R, Jackowski S (2007) Biosynthesis of pantothenic acid and coenzyme A. EcoSal Plus 2(2)
Lin JH, Yamazaki M (2003) Role of P-glycoprotein in pharmacokinetics: clinical implications. Clin Pharmacokinet 42(1):59–98
Lin K, Tibbitts J, Shen BQ (2013) Pharmacokinetics and ADME characterizations of antibody-drug conjugates. Methods Mol Biol (Clifton NJ) 1045:117–131
Lionta E, Spyrou G, Vassilatis DK, Cournia Z (2014) Structure-based virtual screening for drug discovery: principles, applications and recent advances. Curr Top Med Chem 14(16):1923–1938
Lipinski CA (2004) Lead- and drug-like compounds: the rule-of-five revolution. Drug Discov Today Technol 1(4):337–341
Lipinski CA, Lombardo F, Dominy BW, Feeney PJ (2001) Experimental and computational approaches to estimate solubility and permeability in drug discovery and development settings. Adv Drug Deliv Rev 46(1–3):3–26
McMurry JE, Ballantine DS, Hoeger CA, Peterson VE (2017) Fundamentals of general, organic and biological chemistry. Pearson Education, Limited, London
Meduru H, Wang Y-T, Tsai JJP, Chen Y-C (2016) Finding a potential dipeptidyl peptidase-4 (DPP-4) inhibitor for type-2 diabetes treatment based on molecular docking, pharmacophore generation, and molecular dynamics simulation. Int J Mol Sci 17(6):920
Mortelmans K, Zeiger E (2000) The Ames salmonella/microsome mutagenicity assay. Mutat Res 455(1–2):29–60
Nguyen KD, Pan Y (2013) A knowledge-based multiple-sequence alignment algorithm. IEEE/ACM Trans Comput Biol Bioinf 10(4):884–896
Onyango R (2011) State of the globe: tracking tuberculosis is the test of time. J Glob Infect Dis 3(1):1–3
Overington JP, Al-Lazikani B, Hopkins AL (2006) How many drug targets are there? Nat Rev Drug Discov 5(12):993–996
Petrova SS, Solov'ev AD (1997) The origin of the method of steepest descent. Hist Math 24(4):361–375
Pradhan S, Sinha C (2017) Combating prostate cancer bysulfonamide compounds: Theoretical prediction. J Indian Chem Soc 94(10):1113–1122
Rauk A (1994) Orbital interaction theory of organic chemistry. Wiley, Amsterdam
Roncaglioni A, Toropov AA, Toropova AP, Benfenati E (2013) In silico methods to predict drug toxicity. Curr Opin Pharmacol 13(5):802–806
Rozhenko AB (2014) Density functional theory calculations of enzyme-inhibitor interactions in medicinal chemistry and drug design. In: Gorb L, Kuz'min V, Muratov E (eds) Application of computational techniques in pharmacy and medicine. Springer, Dordrecht, pp 207–240
Sangeetha Gowda KR, Mathew BB, Sudhamani CN, Naik HSB (2014) Mechanism of DNA binding and cleavage. Biomed Biotechnol 2(1):1–9
Sanguinetti MC, Tristani-Firouzi M (2006) hERG potassium channels and cardiac arrhythmia. Nature 440(7083):463–469
Sievers F, Higgins DG (2014) Clustal omega, accurate alignment of very large numbers of sequences. Method Mol Biol (Clifton NJ) 1079:105–116
Sirajuddin M, Ali S, Badshah A (2013) Drug–DNA interactions and their study by UV-Visible, fluorescence spectroscopies and cyclic voltametry. J Photochem Photobiol B 124:1–19
Soga S, Shirai H, Kobori M, Hirayama N (2007) Use of amino acid composition to predict ligand-binding sites. J Chem Inf Model 47(2):400–406
Stefańska J, Antoszczak M, Stępień K, Bartoszcze M, Mirski T, Huczyński A (2015) Tertiary amides of Salinomycin: a new group of antibacterial agents against *Bacillus anthracis* and methicillin-resistant *Staphylococcus epidermidis*. Bioorg Med Chem Lett 25(10):2082–2088
Strom ET, Wilson AK (2013) *Pioneers of quantum chemistry*. Am Chem Soc vol 1122
Szymański P, Markowicz M, Mikiciuk-Olasik E (2012) Adaptation of high-throughput screening in drug discovery—toxicological screening tests. Int J Mol Sci 13(1):427–452
The sulfa derivatives in the treatment of tuberculosis (1944) Can Med Assoc J 51(5):467
Trott O, Olson AJ (2010) AutoDock Vina: improving the speed and accuracy of docking with a new scoring function, efficient optimization and multithreading. J Comput Chem 31(2):455–461
Uttamsingh V, Lu C, Miwa G, Gan LS (2005) Relative contributions of the five major human cytochromes P450, 1A2, 2C9, 2C19, 2D6, and 3A4, to the hepatic metabolism of the proteasome inhibitor bortezomib. Drug Metab Dispos Biol Fate Chem 33(11):1723–1728
Vallari DS, Rock CO (1985) Isolation and characterization of *Escherichia coli* pantothenate permease (panF) mutants. J Bacteriol 164(1):136–142
von Delft F, Lewendon A, Dhanaraj V, Blundell TL, Abell C, Smith AG (2001) The crystal structure of *E. coli* pantothenate synthetase confirms it as a member of the cytidylyltransferase superfamily. Structure 9(5):439–450
Vyas VK, Ghate M, Goel A (2013) Pharmacophore modeling, virtual screening, docking and in silico ADMET analysis of protein kinase B (PKB beta) inhibitors. J Mol Graph Model 42:17–25
Wang S, Eisenberg D (2003) Crystal structures of a pantothenate synthetase from *M. tuberculosis* and its complexes with substrates and a reaction intermediate. Protein Sci A Publ Protein Soc 12(5):1097–1108
Wermuth CG, Ganellin CR, Lindberg P, Mitscher LA (1998) Glossary of terms used in medicinal chemistry (IUPAC recommendations 1998). Pure Appl Chem 70:1129
White EL, Southworth K, Ross L, Cooley S, Gill RB, Sosa MI, Manouvakhova A, Rasmussen L, Goulding C, Eisenberg D, Fletcher TM 3rd (2007) A novel inhibitor of *Mycobacterium tuberculosis* pantothenate synthetase. J Biomol Screen 12(1):100–105
Wu G, Robertson DH, Brooks CL 3rd, Vieth M (2003) Detailed analysis of grid-based molecular docking: a case study of CDOCKER-A CHARMm-based MD docking algorithm. J Comput Chem 24(13):1549–1562
Yang SY (2010) Pharmacophore modeling and applications in drug discovery: challenges and recent advances. Drug Discov Today 15(11–12):444–450
Yildiz I, Ertan T, Bolelli K, Temiz-Arpaci O, Yalcin I, Aki E (2008) QSAR and pharmacophore analysis on amides

against drug-resistant *S. aureus*. SAR QSAR Environ Res 19(1–2):101–113

Zhang L, Brett CM, Giacomini KM (1998) Role of organic cation transporters in drug absorption and elimination. Annu Rev Pharmacol Toxicol 38:431–460

Affiliations

Sayantan Pradhan[1] · Chittaranjan Sinha[1]

✉ Chittaranjan Sinha
crsjuchem@gmail.com

Sayantan Pradhan
sayan23us@gmail.com

[1] Department of Chemistry, Jadavpur University, Kolkata, West Bengal, India